Multi-echo fMRI

NeuroImage 154 (2017) 59–80

Contents lists available at ScienceDirect

NeuroImage

journal homepage: www.elsevier.com/locate/neuroimage

Multi-echo fMRI: A review of applications in fMRI denoising and analysis of BOLD signals

Prantik Kundu[a,*], Valerie Voon[b], Priti Balchandani[a], Michael V. Lombardo[c], Benedikt A. Poser[d], Peter A. Bandettini[e]

[a] Departments of Radiology and Psychiatry, Icahn School of Medicine at Mount Sinai, New York, NY, USA
[b] Behavioral and Clinical Neuroscience Institute, University of Cambridge, Cambridge, UK
[c] Department of Psychology and Center for Applied Neuroscience, University of Cyprus, Nicosia, Cyprus
[d] Department of Cognitive Neuroscience, Maastricht University, Maastricht, NL, The Netherlands
[e] Section on Functional Imaging Methods, National Institute of Mental Health, Bethesda, MD, USA

ABSTRACT

In recent years the field of fMRI research has enjoyed expanded technical abilities related to resolution, as well as use across many fields of brain research. At the same time, the field has also dealt with uncertainty related to many known and unknown effects of artifact in fMRI data. In this review we discuss an emerging fMRI technology, called multi-echo (ME)-fMRI, which focuses on improving the fidelity and interpretability of fMRI. Where the essential problem of standard single-echo fMRI is the indeterminacy of sources of signals, whether BOLD or artifact, this is not the case for ME-fMRI. By acquiring multiple echo images per slice, the ME approach allows T_2* decay to be modeled at every voxel at every time point. Since BOLD signals arise by changes in T_2* over time, an fMRI experiment sampling the T_2* signal decay can be analyzed to distinguish BOLD from artifact signal constituents. While the ME approach has a long history of use in theoretical and validation studies, modern MRI systems enable whole-brain multi-echo fMRI at high resolution. This review covers recent multi-echo fMRI acquisition methods, and the analysis steps for this data to make fMRI at once more principled, straightforward, and powerful. After a brief overview of history and theory, T_2* modeling and applications will be discussed. These applications include T_2* mapping and combining echoes from ME data to increase BOLD contrast and mitigate dropout artifacts. Next, the modeling of fMRI signal changes to detect signal origins in BOLD-related T_2* versus artifact-related S_0 changes will be reviewed. A focus is on the use of ME-fMRI data to extract and classify components from spatial ICA, called multi-echo ICA (ME-ICA). After describing how ME-fMRI and ME-ICA lead to a general model for analysis of fMRI signals, applications in animal and human imaging will be discussed. Applications include removing motion artifacts in resting state data at subject and group level. New imaging methods such as multi-band multi-echo fMRI and imaging at 7 T are demonstrated throughout the review, and a practical analysis pipeline is described. The review culminates with evidence from recent studies of major boosts in statistical power from using multi-echo fMRI for detecting activation and connectivity in healthy individuals and patients with neuropsychiatric disease. In conclusion, the review shows evidence that the multi-echo approach expands the range of experiments that is practicable using fMRI. These findings suggest a compelling future role of the multi-echo approach in subject-level and clinical fMRI.

Introduction

Blood oxygenation level dependent (BOLD) functional MRI (fMRI) is widely used to study brain activity based on hemodynamic signals (Bandettini et al., 1992; Bullmore et al., 1996; Buxton et al., 1998; Friston et al., 1995; Ogawa et al., 1990). However, recent studies show that fMRI data can be severely affected by artifacts (Power et al., 2012). These artifacts relate to subject head motion, cardiac and respiratory effects, and hardware (Glover et al., 2000; Jo et al., 2010). Studies on the effects of fMRI artifacts have brought into question many of the compelling findings on brain function based on fMRI, for example, relating to human brain development (Fair et al., 2009). fMRI artifacts also reduce the statistical power of fMRI studies and lead to spurious findings, which has been associated with a crisis of confidence in fMRI

* Corresponding author.

http://dx.doi.org/10.1016/j.neuroimage.2017.03.033
Accepted 16 March 2017
Available online 29 March 2017

research (Button et al., 2013). Thus, while in recent years the field of fMRI research has both enjoyed advanced technology and expanded use, it also deals with a deep discomfort related to many known and unknown effects of artifact. In this review, we discuss an emerging fMRI approach, called multi-echo (ME)-fMRI, which focuses on improving the fidelity of fMRI signals through a physically-driven determination of the origins of fMRI signals as arising from either BOLD contrast or artifact. We also discuss how ME methods can be combined with emerging multi-band acceleration methods to create fMRI strategies with both high resolution and fidelity. Altogether, it is shown that ME-fMRI involves a few relatively small changes from standard fMRI acquisition technique, but enables analyses that support major improvements in fMRI data quality.

To date, the challenges in controlling fMRI artifacts have been met with generic time series signal processing methods such as regression and frequency-restricting bandpass filters (Satterthwaite et al., 2012). Head motion artifacts, modeled from shifts in brain images over time, are regressed out of fMRI time series. Recordings of physiology during MRI are used to model cardiac and respiratory artifact regressors (Glover et al., 2000). Spontaneous activity is band pass filtered to retain a narrow range of frequencies in order to exclude hardware related signal drifts and high-frequency noise (Carp, 2013). Time series models of noise and usually their temporal derivatives are linearly regressed out of data. Despite the significant reduction in information in data after applying these steps, it is now clear that much artifact remains. Of late, simple deletion of volumes from fMRI datasets has been suggested (Power et al., 2012). This altogether means that artifact signals are not characterized well enough by modeling artifact time courses and regressing them out of data. This reality also suggests that artifacts are themselves various and complex, and may interact in unpredictable ways. At the heart of the issue, however, is that standard fMRI approaches do not have a strong and general ground truth to precisely relate signals to biophysical signal mechanisms versus artifacts. Given information on how signals scale across the echo images of an ME-fMRI experiment, however, valuable insight on the origins of fMRI signals in BOLD contrast or artifact can be gained.

ME-fMRI and fMRI relaxometry

After excitation, standard fMRI uses 2-D echo planar imaging to acquire slice images at a single TE, one slice at a time. At 3 T, this TE is usually 30 ms. ME-fMRI uses a slightly different approach. After a normal excitation pulse, a slice image is acquired at the earliest TE possible. Without exciting again, readout of another image of the same slice is then acquired immediately afterward, at a longer TE, and so forth up to the desired number of images and TEs. This happens for each slice of the brain volume. Using this approach, in most cases, there is no cost for acquiring the early TE, since standard fMRI pulse sequences are idle during the early period after excitation. Acquiring extra images after the 'standard' intermediate TE is the main cost. The important benefit is that the T_2* signal decay can be modeled for each voxel. This information can be used to relate signals to their generative physical processes, and can help in mitigating artifacts of many kinds.

Different voxels have different T_2* decay depending on tissue properties and variation of the local magnetic field. These properties can be parameterized based on an ME experiment. ME images can be acquired using 3 T and 7 T MRI (Fig. 1). From ME images, it is seen that early TEs have high signal intensity but a low level of contrast between gray and white matter and CSF. Intermediate TEs have lower average intensity but more contrast. Late TEs have even lower intensity signals, in general, but relatively higher intensity signals in voxels with the slowest decays i.e. longest T_2*values. From ME-fMRI, T_2* relaxometry is made possible, whereby each voxel's T_2*can be estimated from the data based on how signals scale across echoes. One such approach is fitting each voxel's signal values across TEs to a monoexponential decay, shown in Eq. (1).

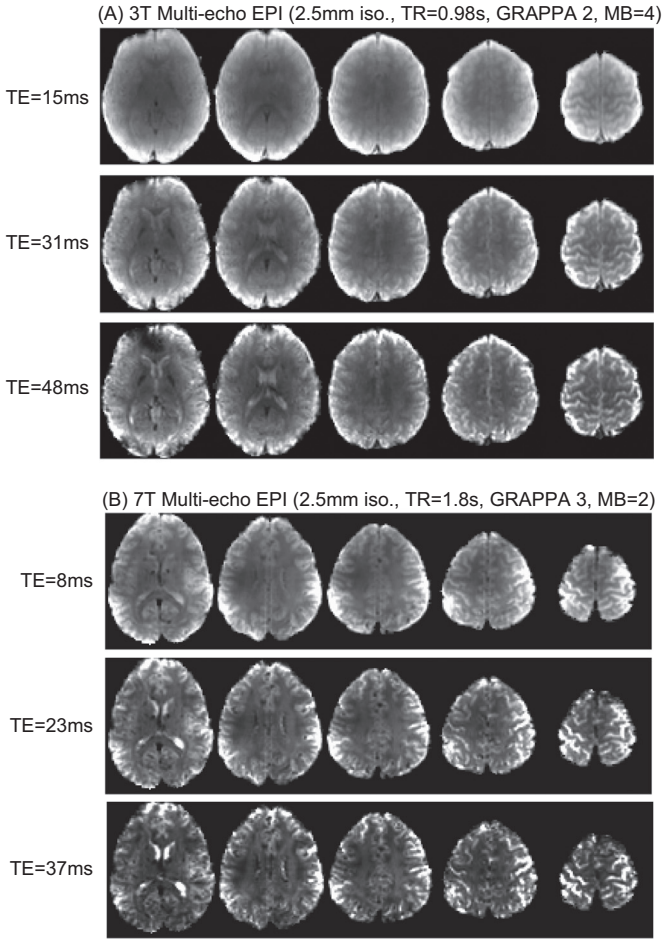

Fig. 1. Multi-echo fMRI images from 3 T and 7 T. (A) 3 T multi-echo images with in-plane and multi-band acceleration with 2.5 mm isotropic resolution and < 1 s TR. (B) 7 T multi-echo images with GRAPPA factor 3 and 2.5 mm isotropic resolution, no multi-band acceleration, giving TR=2.5 s.

$$S(TE) = S_0 \exp(-R_2^* TE) \quad (1)$$

Two parameters are estimated from the fit. One is the decay rate R_2* (reciprocal of time T_2*). The other is S_0, the intercept, also called initial signal intensity. These parameters can be rendered as maps of TT_2* and of S_0 (Fig. 2). The T_2* map reflects tissue oxygenation state. The S_0 map shows coil sensitivity, which is determined by where the head is in the coil and the geometry of the coil elements. S_0 and T_2* may be estimated from just a single volume of fMRI data. Estimates from one volume are noisy, however, so to reduce noise and produce more precise parameter estimates, T_2* and S_0 values can be computed from an average of signals over time. Other approaches to estimating S_0 and T_2* involve incorporating biexponential or sinc decay functions into signal models in order to accommodate partial volume effects. However, more advanced models require more TE signals for high-quality fits (Speck et al., 2001). For signals at a few TEs, and for most applications, a monoexponential signal model is adequate. A log-linear fit is also possible and more computationally efficient versus direct exponential fitting, but some regularization is needed to handle small signal amplitude at long TEs.

As more TEs are acquired, T_2* maps more faithfully reflect anatomy. In particular, gray matter and CSF compartments are better distinguished in T_2* parameter maps than in the original EPI images (Speck et al., 2001; Fig. 3). A 3-compartment image segmentation of a T_2* map can isolate gray matter (Fig. 4a). As the size of ventricles and the subarachnoid space increases, such as with increased age or disease, the boundary between gray matter and CSF becomes more

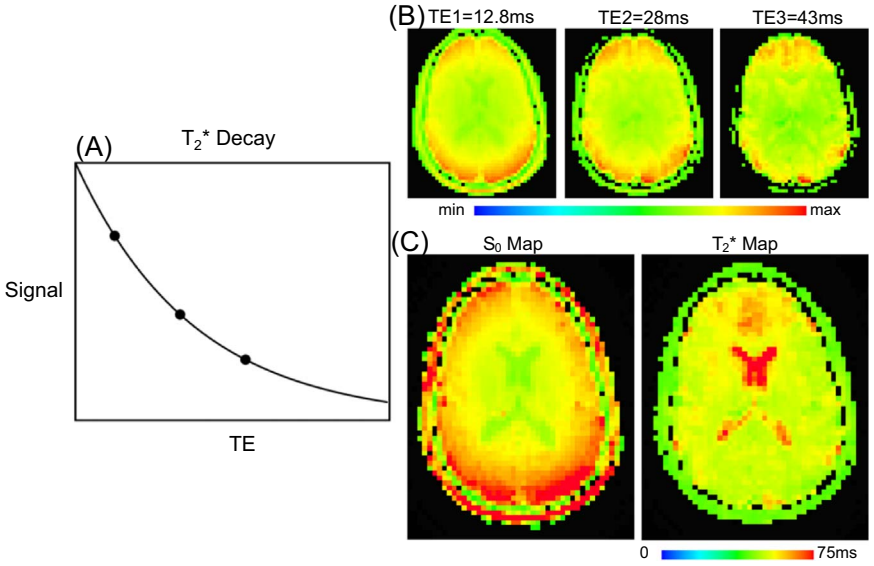

Fig. 2. T_2* relaxometry. (A) T_2* decay based on simple monoexponential decay model in Eq. (1), as function of intercept S_0 and decay time T_2*, inverse of rate R_2*. (B) False color multi-echo EPI images from a 3-TE multi-echo fMRI experiment. (C) Maps of parameters S_0 and T_2*. (For interpretation of the references to color in this figure legend, the reader is referred to the web version of this article).

ambiguous in single-TE EPI images. This is a problem when using standard fMRI in aligning functional data to an anatomical image – an important step for mapping functional images to high-resolution anatomy. Using ME-fMRI, the T_2* map can be used to drive anatomical-functional coregistration. By applying a recent edge-based alignment technique called local Pearson correlation (Saad et al., 2009) to T1-weighted anatomical images and the gray matter compartment segmented from T_2* images, an accurate coregistration of structural and functional images can be computed (Fig. 4b).

A voxel's T_2* value determines not only its signal intensity scaling with TE, but also indicates the TE at which the largest amplitude signal change due to BOLD contrast is detected (Fig. 5). When brain activation occurs within a voxel, an influx of oxyhemoglobin increases the homogeneity of the enclosed local magnetic field. This slows down relaxation, so during activation, R_2*.is lower (and T_2* is higher). Taking the difference of two signal decays corresponding to different R_2*. values shows how signal contrast varies with TE, called a contrast curve. T_2* varies considerably over the brain, such that the optimal TE for best BOLD contrast is actually region-dependent. At 3 T, motor and visual cortices have T_2* around 40–60 ms (Bandettini et al., 1994). Orbitofrontal and inferior temporal cortices have T_2* of about 20 ms due to closeness to the tissue-air boundaries of sinuses. This proximity creates magnetic gradients in the nearby areas, leading to image artifacts associated with magnetic susceptibility. At 7 T, T_2* values are approximately halved compared to 3 T and vary more over the brain. This makes selecting a globally optimal TE even more tenuous at 7 T than 3 T. Thus, selecting a single TE for fMRI gives less than optimal BOLD contrast for most of the brain.

Acquiring images at multiple TEs and combining them is a powerful way to mitigate signal losses in areas with short T_2* while enhancing BOLD contrast throughout the brain (Fig. 6). In a multi-TE acquisition, early TEs have less dropout than later ones. Simply summing signals across echoes increases BOLD contrast-to-noise ratio for TEs up to TE=3.2xT_2*. For regions with short T_2*, a different scheme provides better results, involving a weighted-average based combination of echoes. This combination synthesizes signals that approximate acquisition at the TE~T_2* specific to each voxel, achieved by the combination scheme given in (Posse et al., 1999).

$$w(T_2^*)_n = \frac{TE_n \cdot \exp(-TE/T^*_{2(\text{est})})}{\sum_n TE_n \cdot \exp(-TE/T^*_{2(\text{est})})} \quad (2)$$

w_n is the weight value specific to echo n for a given T_2* value. This approach requires estimating T2* at each voxel, after acquiring multi-TE images, and determining per-TE, per-voxel weights based on T2* values. While this combination scheme is robust, the requirement of per-voxel estimates of T2* could be considered computationally expensive. Other schemes involve per-voxel, per-TE weights without the estimation of T_2*. Using only TE and either signal intensity or signal-to-noise ratio (SNR) to factor the effect of image noise, a different weighting scheme is possible:

$$w(SNR)_n = \frac{SNR_n \cdot TE_n}{\Sigma_n SNR_n \cdot TE_n} \quad (3)$$

The combination of TE signals in the manner of Eq. (3), referred to as parallel-acquired inhomogeneity desensitized (PAID) ME-fMRI, is comparable to that of Eq. (2) given noise is isotropic and homogeneous throughout the image (Poser et al., 2006; Buur et al., 2008, 2009). However, given the high levels of artifact typical in most fMRI data, which adds to variance and thus reduces signal-to-noise ratio, the assumption of isotropic noise may not suitable. In other words, depending on data quality and method of estimation, SNR may not reflect BOLD sensitivity and thus may not lead to optimal BOLD contrast. This condition makes the approach in Eq. (2) an appropriate choice if a T2* map is available. Given the performance of modern computers and numerical computation software, computing per-voxel estimates of T2* and T2*-based weights is not prohibitive after acquiring ME-fMRI data. While the above ME combination schemes reduce susceptibility artifact associated with through-plane air-tissue boundary effects, they do not control in-plane contributions of susceptibility artifact. For better control of the in-plane contribution, a multi-TE sequence that also applies specialized gradient pulses prior to each TE image can be used. The gradient pulses are slice-specific, based on a pre-scan for estimating the phase offsets needed to control the in-plane susceptibility artifact contribution (Deichmann et al., 2002). After considering ease of acquisition and analysis requirements, the method in Eq. (2) offers a good compromise. This approach leads to overall increases in BOLD sensitivity and a level of control over susceptibility artifacts compared to single-echo fMRI that is likely to be well-suited to many current whole-brain fMRI applications.

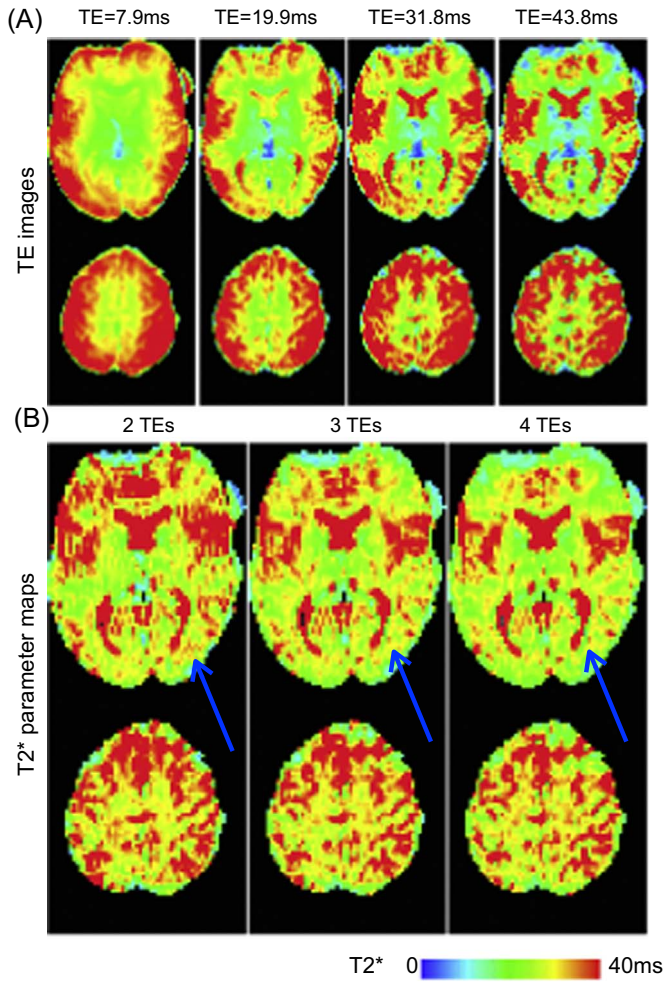

Fig. 3. For multi-echo data acquired at 7 T with 2.5 mm isotropic resolution, (A) TE images in arbitrary units, colorized. Tissue contrast changes with TE, but CSF or gray matter compartments are unclear. (B) Calculation of T_2* maps using 2 to 4 echo images. Using just 2 TE images to generate a T_2* map is informative of CSF localization, emphasized in ventricles (top pane) and in subarachnoid space (bottom pane). However, checkering artifact is present. As more TEs are used for estimating T_2* maps, the influence of artifact on T_2*estimates decreases. The precision of anatomical localization of T_2* values also increases when using more TE images for parameter estimates (arrows).

TE-dependence and TE-independence of signal changes in ME-fMRI data

Managing the contribution of various artifacts such as from subject head motion to fMRI time series is the central problem of fMRI denoising and analysis. When using single-echo fMRI, the challenge is in distinguishing neurally-related activity from artifacts. However, the scaling of fMRI signals across TEs, based on ME-fMRI data, can be analyzed to infer origins in neurally-related versus artifactual signal processes.

The amplitude of a signal fluctuation from standard single-echo fMRI data is usually expressed in terms of percent signal change. However, this amplitude varies depending on the TE with which the signal is acquired with, and the T2* value of the voxel. This effect relates to the contrast curve described earlier (Bandettini et al., 1994; Menon et al., 1995; Posse et al., 1999). For instance, in an experiment using a typical behavioral paradigm imaged at systematically varying TE values, percent signal changes of activation scale with TE. In other words, an activation magnitude could be 1.0% at TE=10 ms, 2.0% at TE=20 ms, and 3.0% and TE=30 ms, and so forth (Bandettini et al., 1994). Resting state fMRI time series also exhibit the same effect (Peltier and Noll, 2000). The finding of TE-dependent scaling in resting state signals was supportive evidence to indicate that resting state activity was related to BOLD signals and not to non-BOLD artifact. Peltier and Noll, in their important study, demonstrated the TE-dependent scaling of resting state fMRI signals averaged from the time series of the hand area of the motor cortex and the scaling of its connectivity to other brain regions in the motor cortex network. Fitting a normalized seed time series to the time series of all voxels of the brain, for each TE, showed significant linear TE-dependent scaling, indicating a T2* effect. These experiments showed that the scaling of fMRI percent signal change with TE could be a general indicator of signals arising from the BOLD contrast. Such insights about the physical origins of fMRI signals could be made without limits on the properties of the signal time course such frequency profile (Chen and Glover, 2015).

While BOLD fMRI signals are considered to represent changes in T2*, in reality, they also reflect changes in S_0 (Gowland and Bowtell, 2007), which underlie artifacts. S_0 changes must be removed in order to achieve clean fMRI signal, which is in principle the objective of fMRI denoising methods. For single-echo fMRI, this is done by generic time series signal processing such as by using regression of noise models and frequency-based filtering methods. For multi-echo fMRI, removal of S_0 artifacts can be done with approaches based on relaxometry. Whereas T2* changes arise chiefly from changes in tissue oxygenation, changes in S_0 arise from many other processes, but can be generally thought to arise from changes over time in the “spin density” of the tissue being imaged in a voxel. Changes in T_2* and S_0 affect fMRI signals approximately independently (Zhao et al., 2006). In practice, the cerebrovascular hemodynamics of blood oxygenation and thus T_2* also change blood flow and volume and thus modulate S0 somewhat. However, BOLD-related changes modulate T_2* much more substantially than S_0, making S_0 change a specific indicator of artifacts. The physical processes that directly affect S_0 change include head motion, fluctuations related to MRI hardware, cerebrospinal fluid, and cerebrovascular pulsatility. Taking all these relationships into consideration, fMRI signals with a high T_2* and a low S_0 contribution are most likely to relate to changes in blood oxygenation and thus functional brain activity. All other signals are associated with artifacts, which can be modeled as having high S_0 contribution, irrespective of their T_2* contributions.

An early application of decomposing fMRI signals into T_2* and S_0 parameter series involved fitting ME signals of each voxel at each time point to the exponential decay model of Eq. (1) (Bright and Murphy, 2013; Ing and Schwarzbauer, 2012; Speck and Hennig, 1998). An important demonstration was that S_0 parameter time series captured artifactual signal drifts, which relate to slow head motion and the heating of MRI gradients over an experiment, while T_2* parameter time series did not show drift. However, time series of T_2* and S_0 parameters computed from sample-by-sample fits of signals to Eq. (1) are noisy, at the least because of the noise in individual fMRI signal measurements (Krüger and Glover, 2001). So, direct T_2* and S_0 fitting are good for separating low-frequency BOLD signals from noise, but not for capturing T_2* modulation of higher frequency BOLD signals that could alias with variations from fit error. High-frequency BOLD signals are important. They are created by event-related tasks, and in decomposition-based analyses such as independent component analysis (ICA), are needed as detail to disentangle functional networks from each other and from high-frequency artifacts related to the cardiac cycle. High noise sensitivity also limits T_2* and S_0 fitting for signals in areas with low signal-to-noise ratios such as the basal ganglia and the brainstem. Attempting to compensate for noise in sample-by-sample S_0 and T_2* estimation by acquiring signals at more TEs changes the repetition time of an fMRI experiment. This again limits sensitivity to higher frequency effects. However, direct T_2* fitting remains attractive for its simplicity, so retaining some sensitivity to higher frequency activity may be handled by computing T_2* fits with frequency-specific

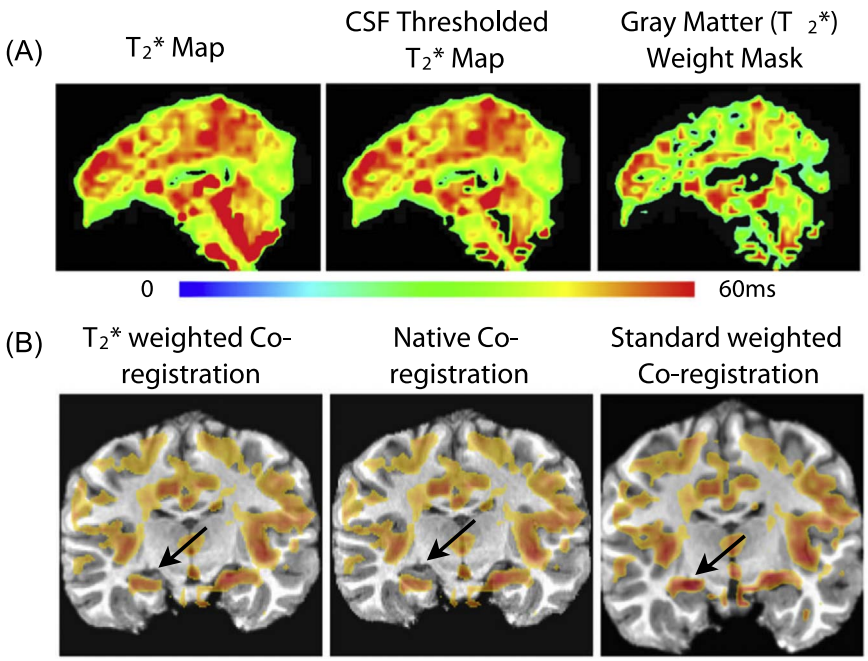

Fig. 4. A representative case of using T_2*maps to drive anatomical-functional coregistration. (A) T_2* map generated from multi-echo fMRI data. The T_2* map is thresholded to mask out CSF, by modeling CSF as having twice the T_2* of gray matter. This masked T_2* map is segmented, to generate a T_2* weight mask for driving anatomical-functional segmentation. (B) T_2* weighted coregistration uses local Pearson correlation to estimate an affine warp. The weight maps show high intensity in gray matter, including hippocampus. Native coregistation (i.e. rigid-body) mis-registers subcortical areas. Standard affine warp based on global estimate overscales the anatomical image.

regularization. For example, a secondary weighting as could be applied in T_2* fitting after a Fourier or wavelet transformation (Bullmore et al., 2004).

fMRI signals that are expressed in terms of signal changes from a mean signal can also be used to compute the change in T_2*, dT_2*, and the change in S_0, dS_0. For convenience, the relaxation time T_2* is expressed here as the inverse of the relaxation rate, R_2*. The signal change model is expressed in the expanded exponential decay equation:

$$\overline{S} + \Delta S = (\overline{S_0} + \Delta S_0) e^{-(\overline{R_2^*} + \Delta R_2^*)\cdot TE)} \tag{4}$$

Eq. (4) is an expansion of Eq. (1) that explains a modulated signal $\overline{S} + \Delta S$ in terms of $\overline{S_0} + \Delta S_0$ and $\overline{R_2^*} + \Delta R_2^*$ (Menon et al., 1995). The direct exponential fitting of signal values to this model is not computationally efficient, which limits its application to large fMRI datasets. However, a Taylor series expansion (shown up to 4 terms) provides a linear approximation for fMRI percent signal changes, $\Delta S/\overline{S}$, that can be used to solve for the changes ΔR_2* and ΔS_0:

$$\frac{\Delta S}{\overline{S}} = \left[\frac{\Delta S_0}{\overline{S_0}} - \Delta R_2^*\cdot TE\right] + \left[\frac{(\Delta R_2^*\cdot TE)^2}{2} + \frac{\Delta S_0\cdot(\Delta R_2^*\cdot TE)^2}{2\overline{S_0}}\right] + \ldots \tag{5}$$

The first linear term shows that percent signal changes have a component due to changes in S_0, ΔS_0, that depend on the baseline S_0 alone. The second linear term shows that a component of percent signal change due to R_2*, dR_2*, is dependent on TE alone (Fig. 7). This suggests that signal changes due to R_2* (i.e. T2*) and S_0 may be separable from each other. These correspond to TE-independent and TE-dependent signal changes, respectively. The TE-dependence term can be used as a model to estimate dR_2*. It is of note that some approximation error could be incurred when using this model. However, fMRI signal changes up to about 50% can yield accurate estimates of dR_2* (Kundu et al., 2011). By comparison, signal changes due to brain activation are on the order of about 1%, and so can be used to estimate dR_2* with good accuracy. The third and fourth linear terms, expanded from the second term of the Taylor expansion, explain residual signal variance that is not explained by the TE-independence and TE-dependence models. The last linear term shows the first component where simultaneous changes ΔS_0 and ΔR_2* interact. However, only large changes in both these terms, larger than any conventional BOLD percent signal change due to functional activity, will create percent signal changes by this mechanism. In summary, percent signal changes can be explained in terms of the separated TE-dependence and TE-independence terms, respectively:

$$\frac{\Delta S}{\overline{S}} = -\Delta R_2^*\cdot TE$$
$$\frac{\Delta S}{\overline{S}} = \frac{\Delta S_0}{\overline{S_0}} \tag{6}$$

This means that irrespective of conditions such as MRI field strength, TE-dependence and TE-independence terms can explain how fMRI signal changes relate to either a BOLD T_2* change or an artifactual S_0 change. The linear separability of the terms means that TE-dependence and TE-independence models can be fit separately to the same sets of percent signal changes to determine which of the two models better explains those signal changes.

Classifying statistical components of fMRI datasets as problem and opportunity

TE-dependence and TE-independence models can be applied to classify signal components of fMRI that are found using spatial independent component analysis (ICA) (Kundu et al., 2012). ICA is a powerful method that can factor fMRI image time series into a set of linearly separable component maps and their corresponding time courses, expressed as

$$X(v, t) = A(v, c)\cdot w(c, t) \tag{7}$$

where X is a voxel-by-time matrix of time series, A is a voxel-by-component matrix expressing spatial maps, and W is a component-by-time matrix of the time series representing the modulation of the maps over time. ICA is designed to find component maps in multivariate data that are maximally distinct from each other in terms of statistical independence. One metric used to estimate independence is negative entropy, used in InfoMax ICA (Bell and Sejnowski, 1995). Another

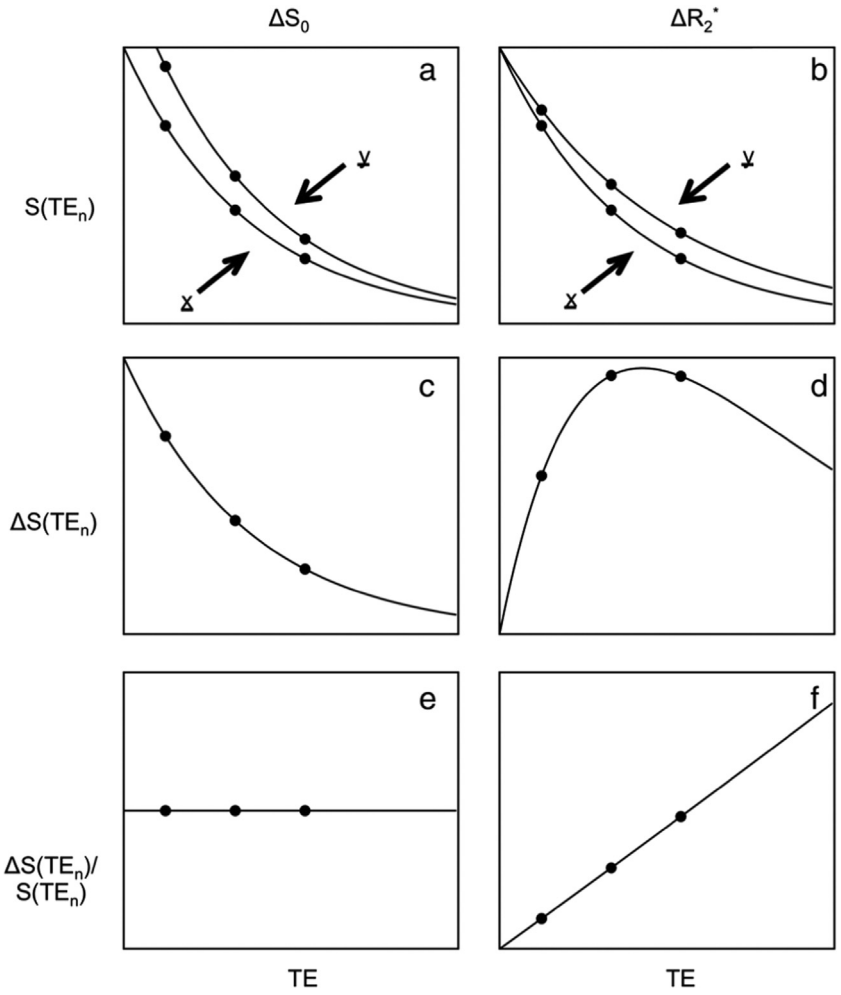

Fig. 5. TE-independence of non-BOLD versus TE-dependence of BOLD fMRI signal changes as underlies artifact and activation, respectively. Exponential decays of signal with TE that differ (a) in intercept S_0 (spin-density), and (b) in decay rate (relaxation rate, due to magnetic susceptibility). Computed difference in signal at different TEs due to (c) artifact-related change in S_0, ΔS_0 and (d) BOLD-related change R_2*, ΔR_2*. Computed difference in percent signal change from mean (e) ΔS_0 and (f) Δ R2* such as due to BOLD contrast.

metric is kurtosis, the fourth standard statistical moment, which is used in the technique called FastICA. The kurtosis approach is more computationally efficient but is still very effective in finding independent components (Hyvarinen, 1999). Consequently, the FastICA technique is well suited to decomposing large datasets (Correa et al., 2007) such as from long-duration experiments with high temporal resolution, and is the primary ICA algorithm in the widely used tool MELODIC, in the FSL suite (Smith et al., 2004).

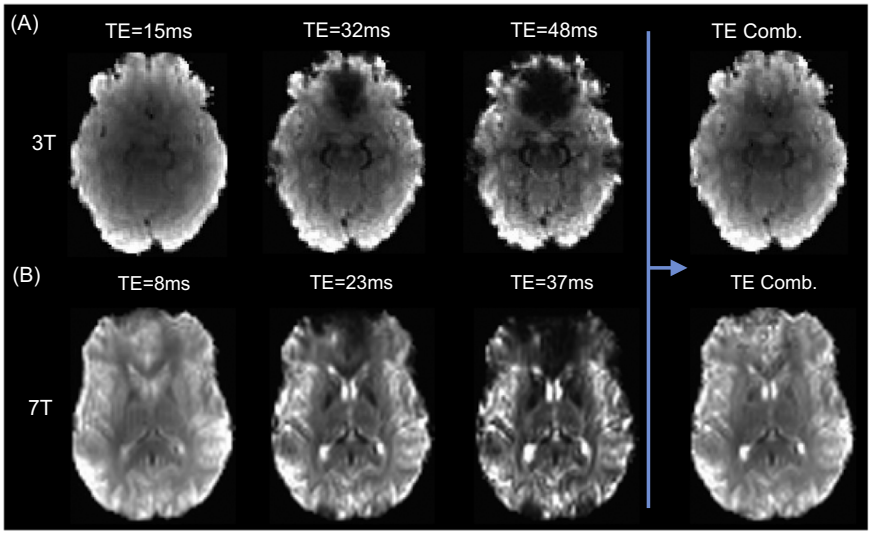

Fig. 6. Combination of echo images from a multi-echo fMRI experiment to give optimally combined image. Signal dropout artifact is due to short T2* in high susceptibility areas, and echo combination weights towards early TE signals in short T2* areas. (A) For images at 3 T (B) and 7 T.

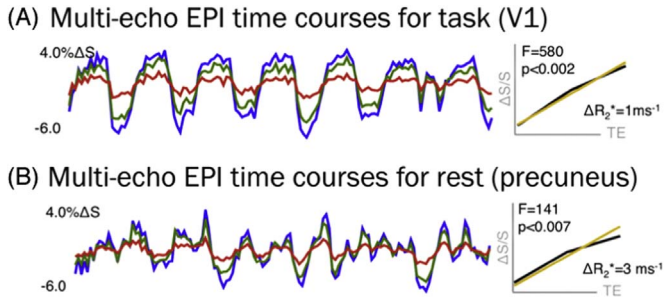

Fig. 7. TE-dependent scaling of BOLD percent signal change during task and rest. (a) Scaling of checkerboard-task related time course from primary visual cortex, showing clear block structure. (b) TE-dependent scaling of resting state signals from precuneus. While resting state time course is not predictable beyond a frequency range, TE-dependent scaling suggests a BOLD effect.

Applying MELODIC ICA to ME-fMRI data results in components with spatial modes resembling functional networks such as the default mode network and artifacts such as pulsation (Fig. 8). Fitting component time series (unit variance) to the different time series of different voxels and TEs showed that for network components, percent signal changes have statistically significant linear scaling with TE, in fitting well to the linear TE-dependence model. Network component signal changes do not fit significantly to the TE-independence constant signal change model. In contrast, many artifact components show constant percent signal change with TE. The significance of fits of signal changes across TEs to scaling models can be determined in terms of F-statistics with degrees of freedom (N_{echo},1), one F-statistic for the TE-dependence model, a separate F-statistic for the TE-independence model. Both F statistics have the same degrees of freedom, so they are numerically comparable to each other. F-statistics were used to threshold the parameter maps of fitting for ΔR_2^* and ΔS_0. Maps of F-statistics, from fitting a few percent signal change values to a slope or a constant line, mirror maps of percent signal change from fitting time

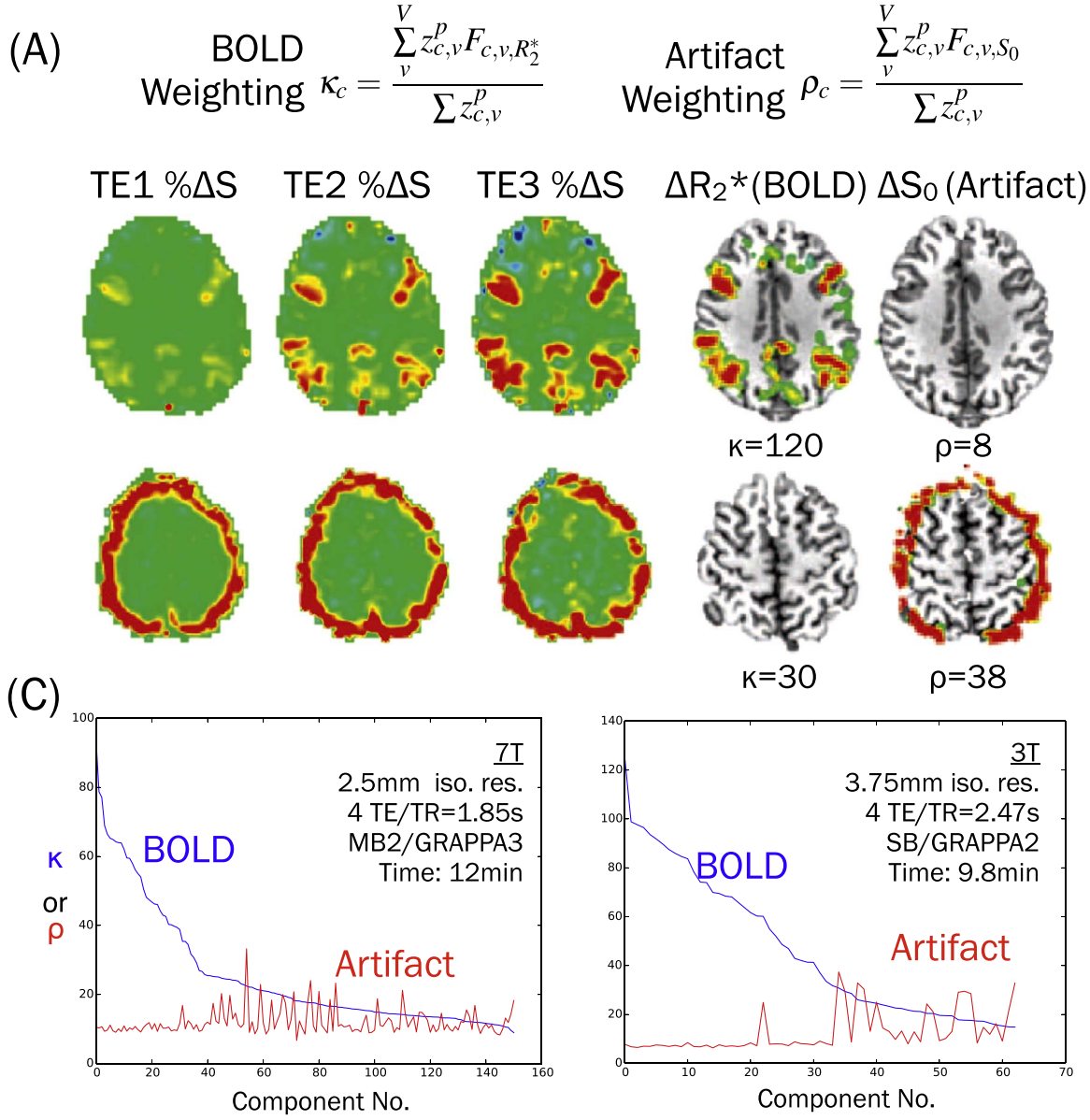

Fig. 8. Multi-echo independent components analysis (ME-ICA). (A) κ and ρ pseudo-F statistics representing component-level TE-dependence and independence, of BOLD and artifact, respectively. (B) In the first three columns, the percent signal changes across TEs, of network and artifact components in top and bottom rows, respectively. The last two columns show parameter maps from fitting percent signal changes to TE-dependence and TE-independence models, thresholded by goodness of fit F_{R2}^* and F_{S0}, respectively. (C) K and ρ spectra, for 7 T and 3 T data.

series of many points to each other. This suggests that the TE-dependence and TE-independence model fitting of ICA component amplitudes is a robust means of inferring the physical sources generating component signals.

Overall weightings for TE-dependence and TE-independence have been proposed to characterize the ICA components given an fMRI dataset (Kundu et al., 2012). Simple averaging of F_{R2}* over each component, and likewise for F_{S0}, do not differentiate components with network maps versus artifact maps. This is because only a small number of component voxels have high signal weights or high TE-dependence or TE-independence – most voxels are not significant. Therefore, a weighted average is used. The weight needs to be a measure of the significance of a voxel. Thus, the Z-maps of components are used to provide weight values, derived from fitting the ICA mixing matrix to the optimally combined dataset. The Z-weighted average of F_{R2}* values of a component is called κ (Fig. 8a). The same for F_{S0} values is called ρ. The Scree plot of κ values representing all the components from a statistical decomposition, with ICA being used here, is called the κ spectrum. Rendering a line plot of ρ values in the same component ordering of the κ spectrum showed the relative TE-dependence versus TE-independence per component. The ICA components of ME-fMRI datasets clearly group into two regimes, one with high κ and low ρ, the other with low κ and/or high ρ (Fig. 8c). In some datasets, the regime difference can be seen in the κ-spectrum alone, relative to a clear elbow. In others, both κ and ρ values need to be considered, which is the standard for determining component origins from ME-fMRI data. High κ component groups include cortical networks that have high percent signal change, as well as those expressing smaller magnitudes such as subcortical components of the putamen. The low κ or artifact component group shows components with pulsatility, motion artifact, and in some cases the sagittal draining vein. These findings reinforce the notion that ICA can find components in fMRI data that relatively cleanly group into network and artifact groups, now based on measures of TE-dependence versus TE-independence, indicating that acquiring multi-echo fMRI data could be a viable approach to the ICA component classification problem. On the other hand, these results demonstrated at least two aspects about resting fMRI data and ICA. First is ICA, despite being a statistical technique, finds biophysically specific modulations. Second, modeling ΔR_2* and ΔS_0 of components identifies two relatively clear regimes of components that separate networks and artifacts (Kundu et al., 2011). This framework was called multi-echo ICA (ME-ICA).

A general model for fMRI time series

ME-ICA showed how brain network components could be grouped apart from artifacts of many kinds without spatial or temporal templates of expected functional effects. While ME-ICA was shown first for human resting-state fMRI data from 3 T MRI, it is in principle more broadly applicable. To denoise fMRI, TE-independent component time series could be regressed out of fMRI time series (McKeown et al., 2005). This approach can be used to denoise ME-fMRI of both task and resting-state activity since both arise from the BOLD contrast. Moreover, given ME-fMRI data, task and resting state can be denoised within the same analysis framework, which standards in contrast to the current need for quite different pipelines for denoising standard fMRI data of these different paradigms. In effect, ME-fMRI and ME-ICA could lead to fMRI study workflows that are at once more practically straightforward and physically principled.

ME-ICA may be applied to any data with T_2* signal fluctuations from BOLD contrast. This suggests application to animal fMRI, for example. Animal brain anatomy, in being less morphologically varied than human brain anatomy in MRI images, makes detecting overlying artifacts more difficult to distinguish from signals of interest. Thus, visually picking networks from ICA of animal fMRI can easily be biased to include artifacts. Separating BOLD and non-BOLD signals in an automatic but principled way based on ME data is thus compelling for animal fMRI. The ME approach could also apply to fMRI at different field strengths, including 7 T as well as 1.5 T. These MRI fields are associated with different fMRI artifacts but signals arise concurring with the same TE-dependence and TE-independence mechanisms. In the same way, multi-band and single-band fMRI could also be analyzed by the same pipeline. This means that ME-fMRI and ME-ICA can constitute a general signal model and processing approach for fMRI time series.

A general model for fMRI data would not involve many assumptions about brain activity or artifact patterns in space or time. In other words, a general fMRI analysis would not need conditioning steps like band pass filtering and spatial smoothing. For instance, in standard fMRI, high pass filtering is usually applied to remove drift, and low pass filtering and spatial smoothing are usually applied to remove randomly distributed noise. A general fMRI model would explain these signals without broadly filtering data to remove drift and noise. This would be very useful in experiments where a stable signal baseline is important, such as in the study of slow effects of pharmacological fMRI or learning tasks. For these experiments, ASL is currently used, but often ASL is not optimal due to complexity in use and low signal to noise ratio of that technique (Aguirre and Detre, 2012; Wang et al., 2011).

In the ME-ICA approach to a general fMRI analysis model, the first step is isolating thermal (i.e. random) noise, which is neither BOLD signal nor non-BOLD artifact and is ambiguous to decomposition methods. This noise exhibits Rician or related Gaussian-like distributions, and its prevalence and specific distribution are determined by the imaging system (Wink and Roerdink, 2006). The proportion of thermal noise in a dataset decreases with field strength and increases with smaller voxel sizes. Thermal noise and BOLD can overlap when the maximum sampling frequency (i.e. Nyquist) is low, as it is for most fMRI studies to date, close to 0.3 Hz and lower (Chen and Glover, 2015). Given that most fMRI acquisition cannot acquire at very high sample rate due to signal-to-noise considerations, time series filtering to remove thermal noise is needed that may, in turn, remove BOLD signals that are informative for separating artifacts and networks from each other. At the same time, over- or underestimating the proportion of thermal noise kept or removed by analysis biases statistics (Bullmore et al., 1996). A general fMRI signal model based on ME-fMRI data would have to precisely handle not just BOLD and non-BOLD signals, but thermal noise as well (Fig. 9).

Principal components analysis (PCA) can be part of a strategy to isolate thermal noise without explicit bias to specific spatial or temporal features of the data (Thomas et al., 2002). PCA factors a dataset into components that show patterns of correlated signals, in such a way that each pattern is decorrelated to the others. Principal components (PCs) can explain both signals and noise and can be recombined to the original data perfectly. In fMRI data, the number of PCs equals the number of imaging volumes (TRs). Interesting signals of biological data, such as from brain activity, tend to be more correlated than random noise. If a dataset is comprised of interesting signals and noise, then most of the interesting signals are represented in a just few components that explain most of the variance. The many remaining ones mostly represent noise, and each explains a small and similar amount of variance. PCs are ranked by the percent of variance they explain in the data. Plotting ranked PCA variances makes a Scree plot that usually shows a 'knee' or inflection separating a small number of high variance components from many low variance ones. Components can be grouped into high and low variance groups around this knee in an effort to separate signals and noise. However, knees vary smoothly, which makes a clear cut difficult. Additionally, ranked PCA variances always show a knee, even from PCA of random data, due to random correlations. Therefore, more information is needed in order to precisely capture thermal noise.

Insights from models on signals of interest can be used to better

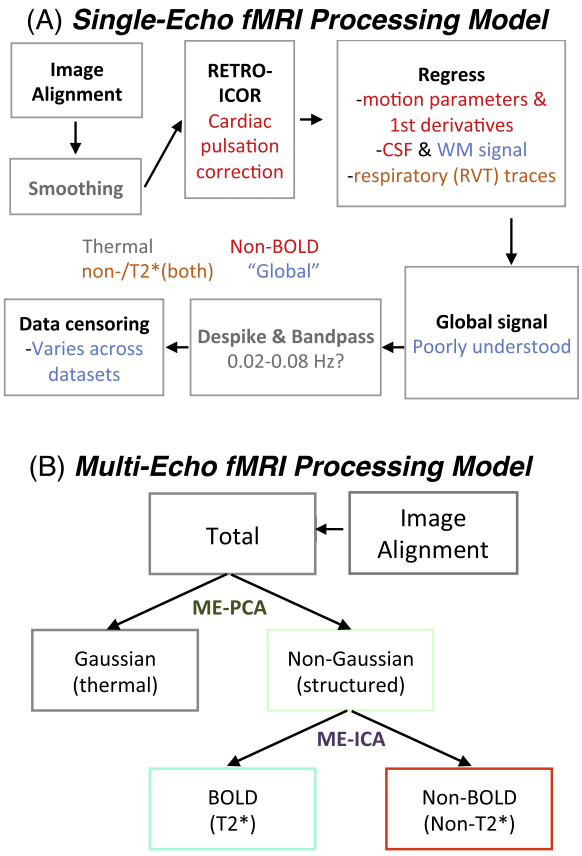

Fig. 9. Comparison of signal processing models for single-echo and multi-echo fMRI data. (A) Single-echo processing steps indicate nuisance types to be modeled. (B) Multi-echo processing based on two steps, ME-PCA and ME-ICA, that separate thermal noise, BOLD and non-BOLD signals.

understand thermal noise. In the PCA step in the popular probabilistic ICA method, it is assumed that BOLD signals have autocorrelated (e.g. repeating or self-similar) fluctuations over time (Beckmann and Smith, 2004). The signals remaining after filtering out autocorrelation are used as a model for random noise. Three steps are used to condition data with this information. The correlation patterns of this noise are first projected out from the correlation patterns of autocorrelated data. Then, variances from PCA of the resulting dataset are normalized by the variances expected of a random dataset of the same size. Last, the number of signal PCs is estimated as the rank where the variance of a data PC is most likely different than the variance of the corresponding noise PC. The likelihood of optimality for a particular PCA rank is estimated using a variety of Bayesian functions. This approach clearly and consistently marks a "reasonable" number of PCs as related to signal. Often, this number is much lower than the number of data volumes, making it a low estimate of "dimensionality". This approach leads to stable ICA solutions, whereby many different types of fMRI data lead to very comparable brain network maps. The noise model does involve some assumptions about brain activity in space and time, but these are reasonable and applicable to many types of data. The performance of probabilistic ICA sets a standard in terms of speed and stability, and biological meaning in results.

κ and ρ metrics that were first used to separate BOLD and non-BOLD ICA components can also be used to model signal and noise based on PCA (Kundu et al., 2013). For instance, this approach can use TE-dependence and TE-independence to help to assess if low-rank PCs are only noise, or if they also represent signals. An interesting case is if a PC captures a rare signal that explains little variance and thus ranks among noise PCs. Removing noise PCs based on a rank cut-off would also remove signal PCs such as these. If these components are not removed, however, their information on a sparse event might lead to better ICA unmixing. Recent evidence shows that low dimensional ICA components showing artifact patterns may not be fully unmixed from network signals (Bright and Murphy, 2015). When these supposed noise components are recomposed into time series, known brain networks can still be seen in their correlations. Using these artifact components to denoise data is then likely to remove network signals. Another caveat is in that given presence of one or few very high variance PCs, such as from drift, probabilistic estimates of dimensionality can be severely low. Analyzing PCs using κ and ρ may help solve these problems. These statistics do not depend on the variance explained by components for inferring component origins (Fig. 10). As pseudo-F statistics, κ and ρ are paired with significance (p) are part of inferring whether a PC has signals from TE-dependent ΔT_2^* or TE-independent ΔS_0 fluctuations. In this approach, called ME-PCA, any PC that does not explain significant variance, and does not have either significant κ or ρ, is counted as thermal noise. Crucially, this approach

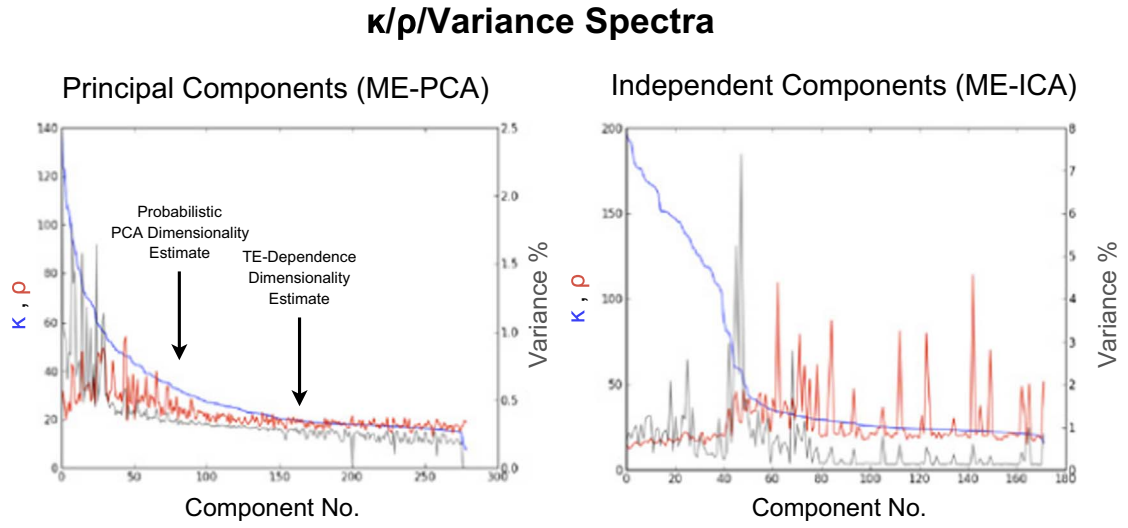

Fig. 10. K and ρ spectra from ME-PCA (left), and from ME-ICA given ME-PCA dimensionality reduction (right). (A) ME-PCA shows that PCA components of fMRI data have coincidentally high K and ρ weights, indicating mixed TE-dependence and TE-independence. This pattern in turn suggests that PCA components of fMRI data have both BOLD and non-BOLD contributions. ME-PCA also shows that PCA components, past a low-dimensional estimate, have detectable MR signals. A higher dimensionality estimate is obtained based on TE-dependence and independence weights (B) ME-ICA unmixing of signals after ME-PCA dimensionality reduction. Two distinct regimes appear, one with high K and low ρ, and the other with vice-versa. These regimes indicate a specifically R_2^* weighted and a non-R_2^* weighted regimes, found in terms of ICA component groups.

to defining signal does not need to group PCs under a certain variance rank as noise. There is also no dependency on temporal or spatial models based on data smoothness, which simplifies the analysis and makes it more general. Any PC with significant signal variance, κ or ρ is classiifed as a signal PC. This is an implementation of PCA that employs a sensitive tertiary measure of signal content in PCs to help determine dataset dimensionality.

Similar in purpose to the PCA step in probabilistic ICA, ME-PCA captures signal PCs from ME data for further unmixing by FastICA. κ and ρ values of PCs show that, unlike components from ICA, PCs have mixed ΔT_2^* and ΔS0 weighting (Fig. 10). Compared to the PCA step of probabilistic ICA, ME-PCA marks on the order of double the number of PCs as related to signal and not noise. ME-PCA includes many PCs with low variance, past the knee of ranked PC variances, and thus leads to solutions with high dimensionality. The performance of ME-PCA in accurately distinguishing signal from noise PCs is demonstrated in the ability of a subsequent FastICA step to stably unmix the dimensionally-reduced data into networks and artifacts. Indeed, FastICA on signal PCs from ME-PCA is stable and has good convergence. This may be considered surprising since a higher dimensionality of data is unmixed than would be the case if using a low-rank dimensionality estimate from probabilistic PCA, for example.

T_2^* weighted combinations of ME-fMRI with a standard resolution (e.g. 3.75 mm resolution) at 3 T can be expected to have 90–95% or more of total data variance decomposed into spatial ICs by ME-ICA. For the same data, probabilistic ICA explains on the order of around 70% of total variance (Kundu et al., 2013). For single-echo fMRI data of the same subjects, probabilistic ICA tends to explain less than 60% of the variance in datasets. κ and ρ scores of ICs from ME-ICA (including ME-PCA) shows good separation of high κ and low ρ components from low κ or high ρ components (Fig. 10b). In general, more BOLD components are found using ME-ICA (and ME-PCA) than probabilistic ICA, in the case of individual subject analysis. Inspecting ME-ICA maps in κ order (from high to low) shows that high κ components are brain networks, but tend to be more regionally specific than lower dimensional ICA results (Fig. 11). For instance, where a low dimensional ICA would show a large-scale motor network, high dimensional ME-ICA is more likely to show separate left and right weighted motor networks. A similar phenomenon is found in visual cortex areas. Notably, fine-grained network mappings have been sought using spatial ICA, but based on datasets combining many runs over a group of subjects, not from one relatively short run of an individual subject. Partly because full-width-half-max (FWHM) smoothing is not applied in ME-ICA preprocessing, network regions elucidated by the ME-ICA pipeline also track anatomy more closely than standard ICA methods. This is achieved despite ME-fMRI data being of imaging resolutions around 3 mm, which is not considered to be a high imaging resolution for fMRI. Subcortical regions are also identified by ME-ICA. These sensitivity gains are achieved without changing equipment or experiment design.

The general model for ME-fMRI data proposed here involves the separation of all data into MR signals and Gaussian noise, and then MR signals into BOLD and non-BOLD sources. This is done using PCA, ICA, and analyses of TE-dependence and TE-independence. As a proof of concept and important application, ME-ICA has been applied to "resting state" fMRI of the rat brain using a Bruker 11.7 T preclinical MRI with a four-channel head coil. This is a challenging application due to imaging with 0.5 mm isotropic resolution voxels as well as anesthesia, which can change neurovascular coupling and BOLD signal (Kundu et al., 2014). After setting the anesthesia protocol and optimizing the ME-fMRI sequence, just one 20-minute scan of one rat could show up to 24 brain networks (Fig. 12). Brain regions and networks were clear, with little if any mixed artifact patterns. Referencing atlases of rat brain anatomy showed that the regions in

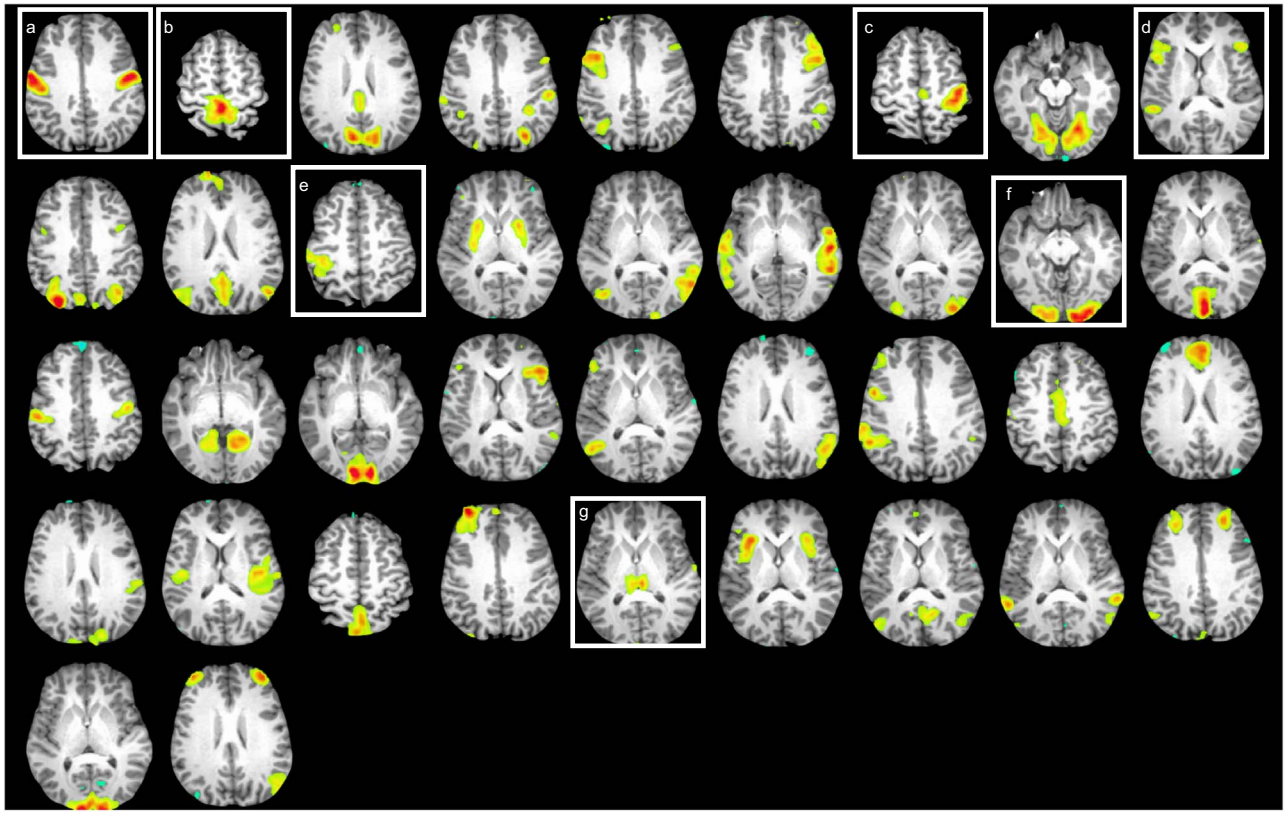

Fig. 11. Components from ME-ICA of a single 10 min. run of resting state ME-fMRI acquired at 3 T using 3.75 mm isotropic voxel size, using ME-PCA dimensionality estimation. Components show: (a) limb representations of motor cortex, (b) foot area, (c) left-lateralized hand area, (d) language network, (e) right-lateralized hand area, (f) primary visual cortex (g) thalamus.

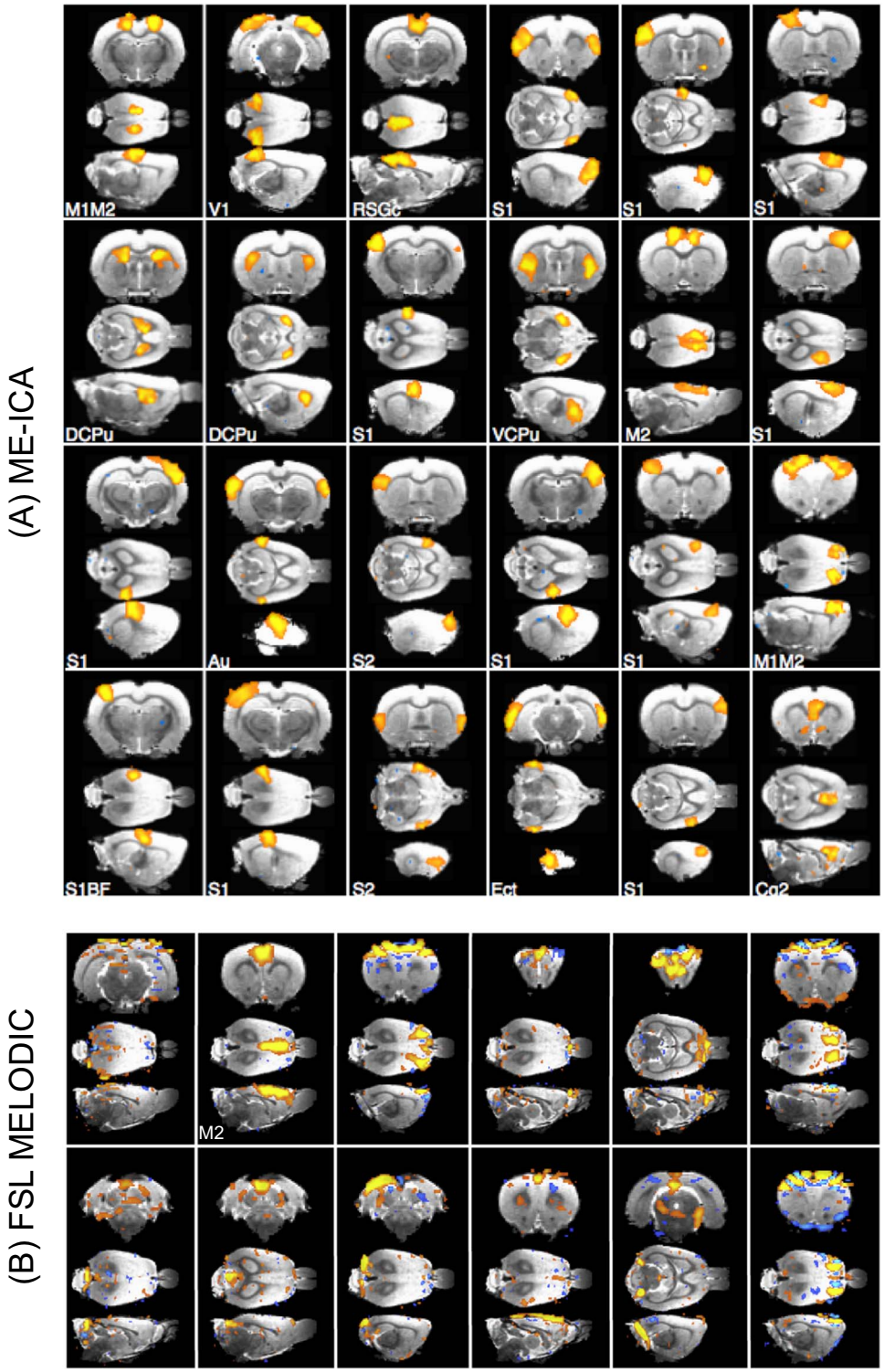

Fig. 12. ICA of spontaneous activity from individual anesthetized rat (under 1% inhaled isoflurane). (A) ME-ICA components show functional networks sharply localized to anatomical regions. These components are ranked based on BOLD weighting. (B) FSL MELODIC shows some comparable BOLD networks, but with ranking based on variance explaining mixing artifacts with networks. FSL MELODIC components show a high degree of mixing between network and artifact patterns.

ME-ICA BOLD networks followed known regional boundaries. These regions were lateralized in many cases, as seen from human resting-state data at 3 T. We compared ME-ICA to probabilistic ICA for these data, which showed fewer ICs overall, fewer networks, and more mixing of networks and artifact patterns. As a second part of the experiment, the level of isoflurane anesthesia was modulated in separate runs. It was found that as inhaled isoflurane was increased from 1% to 2%, the number of BOLD networks decreased significantly. This effect was reproduced across animals. These results showed that ME-ICA and its model for BOLD, non-BOLD signals and noise could improve resting state studies of human, but could also be used to study novel brain function, such as drug manipulations in animals.

One area of component selection where ME information is useful but other information may still be helpful is for susceptibility related dynamic artifacts. These artifacts are signal changes that arise from shifts in the magnetic field over time, such as due to chest motion

during breathing, and other body movements during imaging. These artifacts are likely to have more TE-dependence behavior than other artifacts such as due to head motion and physiological artifacts from changes in blood flow or volume. From ME-ICA, these artifacts tend to manifest with: higher κ than conventionally TE-independent artifacts, lower κ values than functional networks, higher ρ than components of neurally-related BOLD signals (Kundu et al., 2011, Kundu et al., 2013), and typically high levels of variances explained. This pattern suggests mixed T_2* and S_0 origin and is usually found at the 'elbows' of κ spectra. It also follows that these components may be more challenging to disambiguate from functional networks than when using κ and ρ alone.

Sensitivity increases were expected from task-based fMRI analyses on the basis of the considerations made in the general ME-fMRI signal model. These increases were recently demonstrated in a study that characterized the performance of ME-ICA on mapping task-related brain activation at the individual-subject level (Gonzalez-Castillo et al., 2016). The authors applied ME-ICA to data from cardiac-gated block designs, constant repetition time (TR) block designs, and constant TR rapid event-related design. Five different paradigms were utilized to evoke neuronal activity in a distributed set of regions. ME-ICA of this data was compared to more conventional denoising and activation mapping from the middle-echo time series alone and of the T2* weighted combination of echoes. The performance of these analyses were each gauged in terms of activation extent, activation magnitude, percent detected trials and effect size. In cardiac-gated data, ME-ICA reliably detected and removed non-neural T1 signal fluctuations caused by non-constant repetition times. ME-ICA then outperformed the other options in terms of percent detection of individual trials for rapid event-related experiments. These findings suggest that the general ME-ICA signal model leads to a versatile, powerful approach for advanced denoising of task-based fMRI, not just resting-state data. However, the authors noted that only 46% of all events were detected after ME-ICA. This suggested that additional improvements in sensitivity could improve the detection of individual short-event activity. This may be possible by extending the general ME-ICA signal model with an element to manage "global signals," which are high variance spatially distributed fluctuations (Fox et al., 2009; Murphy et al., 2009) that may obscure localized event-related activity. Improved characterization and management of global signals by ME-ICA could lead to further enhancement of sensitivity for event-related designs, but also more generally, such as for resting-state studies.

Future directions include combining TE-dependence information with other component information in the component selection process to identify and remove more challenging artifacts from susceptibility-related dynamic artifacts. Additional characteristics could include component spatial frequencies, which could differentiate spatial patterns of dynamic magnetic field changes versus cortical patterns of functional activity. More robust identification of functional BOLD components versus artifacts could utilize machine learning methods to incorporate more characteristics than κ or ρ alone in the classification process. In keeping with the goal of effective subject-level BOLD/non-BOLD signal separation, components with clear BOLD/non-BOLD attribution based on κ and ρ alone could be used for training a classifier with several more TE-dependence and spatial features, then categorize the remaining components of the same dataset.

Motion artifacts

While motion artifacts have long been known to affect fMRI, only recently has the severity of their impact on studies of connectivity become widely accepted (Power et al., 2012; Satterthwaite et al., 2012). There remains a vital need for an fMRI denoising method that can remove these artifacts in a principled way. Ideally, such a denoising method would lead to improvements in both subject and group levels of study. At the subject level, motion artifacts can either inflate or reduce connectivity. These changes follow patterns of anatomy, covarying for example with the distance between brain areas. At the group level, these errors might not cancel and can accumulate. This is a problem because patients often move more than healthy controls, and controls are often better trained to move less. This leads analyses to show group differences in connectivity, due more to head motion than a neurobiological state. ME-fMRI has previously been shown to help separate out motion artifacts from fMRI data. Examples include T_2* and S_0 fitting, as discussed. Another method involves rescaling amplitudes with T_2* and S_0 weights, then performing ICA (Buur et al., 2008, 2009). Based on the general ME-fMRI model, ME-ICA has been shown to separate out motion artifacts as non-BOLD signals. The use of ME-fMRI and ME-ICA to mitigate motion artifacts has been approached with goals of mitigating both the impact of artifacts on signal time series, as well as spurious connectivity inferences at group level statistical analysis.

ME-ICA produces denoised time series after removing non-BOLD components. To evaluate the impact of motion artifact on ME-fMRI time series, the method of computing DVARS traces can be used, as introduced in Power et al. (2012). A DVARS trace is a single time series that reflects the level of total volume-to-volume signal change over the course of an fMRI run. A high correspondence of DVARS traces with motion regressors indicates strong contributions of motion artifact to fMRI time series. In Fig. 13, DVARS traces are shown for ME-fMRI time series: after T_2* weighted combination only; after standard denoising; and after the split BOLD and non-BOLD time series generated by ME-ICA. Compared to DVARS traces of raw data, standard denoising does not reduce DVARS values. In some conditions, standard denoising seems to overfit noise models and increase DVARS values. Standard denoising is thus indicated to be ineffective for ME data, just as it has for single-echo fMRI data. In contrast, BOLD time series DVARS values are much lower and do not covary as strongly with traces of subject head motion over time. On the other hand, non-BOLD DVARS values closely follow the DVARS traces of raw data. This shows that ME-ICA can sensitively remove motion artifacts. In our study, data from subjects of both high and low movement groups both showed 4-

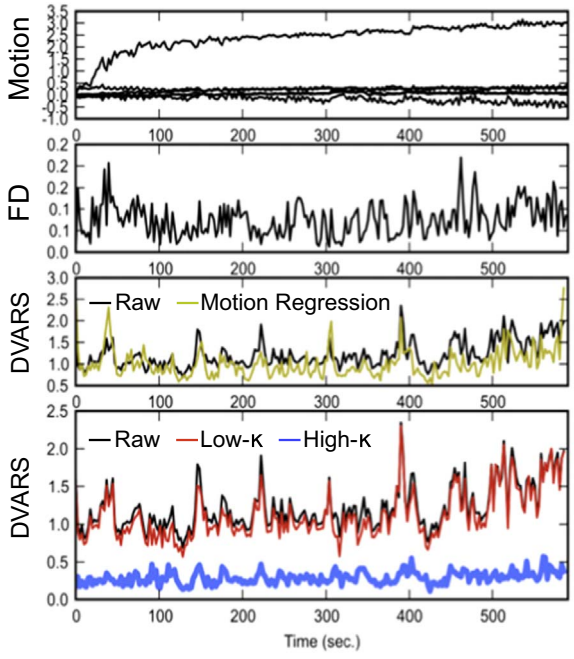

Fig. 13. Comparison of subject motion, signals before and after motion regression, and ME-ICA BOLD (High-K) and non-BOLD (Low-K) time series. The framewise displacement (second panel) matches the DVARS trace of raw data and of motion parameter regressed data (third panel). This pattern suggests that motion regression did not remove the main problematic variance due to motion, with possible indications of overfitting. In contrast, the BOLD time series DVARS is separated from that of the non-BOLD and raw (overlapping), indicating an effective denoising.

fold higher SNR in ME-ICA BOLD time series than in raw data. Where SNR was significantly different in the raw data of these groups, in BOLD time series after ME-ICA, they were not. Of note, the increased SNR after non-BOLD component removal did not result from specifically removing components that reduce SNR but by specifically removing non-BOLD effects.

One important metric in which data from high and low motion subjects have differed is in the number of BOLD components after ME-ICA. While data of these two groups led ME-ICA to explain similar percentages of data variance, the number of BOLD components in high motion data was lower (Kundu et al., 2013). This leads to an insight on the impact of head motion on BOLD signals and connectivity. Firstly of note is that BOLD time series from ME-ICA are made by linearly combining BOLD components. The number of BOLD components is thus equal to the degrees of freedom for correlation of BOLD time series. As degrees of freedom decrease, the range of values of Pearson correlation increases. In group level analysis, as subject groups differ in their average BOLD degrees of freedom, and this is not detected and controlled, connectivity can falsely differ at group level in a similar way. When not accounting for variability in degrees of freedom, statistical errors may arise in the process of comparing correlation values across subject groups with different parameters of subject motion.

The ability to estimate BOLD degrees of freedom at the dataset level affords a means of controlling this variability. A correction can be based on the Fisher R to Z transform. The transform is already a part of standard connectivity analysis, to turn the [−1, 1] R distribution to a normal (Z-distributed) one. However, a truncated Fisher transform is usually used, which drops the degree of freedom factor, as it is assumed to be a constant or random (Hampson et al., 2002). By using the full Fisher transform, Z-values of connectivity result that are better conditioned. Another analysis step towards better conditioning of connectivity is to use series of BOLD independent component (IC) weights and not time series for seed correlations. After simply "stacking" BOLD IC maps into 4-D data, each voxel has a series of weights across corresponding BOLD ICs. IC weights are produced as independent variates, by ICA. In turn, this makes series of IC weights agree more with the assumptions made in tests of significance of correlation leading to valid inference (Fig. 14). Combining these steps results in the method called ME independent components regression (ME-ICR). Maps of seed-connectivity at the subject level based on ME-ICR clearly showed canonical networks at Z values of standard p-values, such as $p < 0.05$ and $p < 0.01$. At the same time, similar connectivity was seen for data of both high and low motion, e.g. low and high degrees of freedom, respectively.

Subject data affected by varying levels of head motion leads to more comparable connectivity maps with ME-ICR than with standard connectivity analysis (Fig. 15a). The impact on group-level connectivity inferences from conditioning subject-level connectivity by degrees of freedom can be assessed using a type I error test and cross-validation (Fig. 15b). The rationale is that a two-sample T-test of seed connectivity maps of the same seed region and groups of subjects without a true difference would yield a null result, meaning that predicted and observed type I error would agree. The expected number of type I errors in a voxelwise test is the expected p-value (i.e. user-defined by the set threshold) times voxel count. The observed type I error is the number of voxels surviving the set threshold. Ideally, the number of observed errors should agree with the number of expected errors, across a range of p-values, for several seed regions, and for various degrees of permuted groupings. The comparison of expected to observed errors in group-level connectivity maps is shown for two group-level connectivity contrasts, one based on ME-ICR subject-level seed connectivity maps, the other based on standard connectivity maps (Fig. 15). In two-sample T-tests of connectivity between randomly drawn groups both standard analysis and ME-ICR show expected levels of type I error. As test groups were increasingly biased to have high versus low levels of subject motion, the standard analysis without control for degrees of freedom showed greater type I error, while ME-ICR did not. In the final and single median-split case of high movers versus low movers, the standard analysis showed double the type I error, while ME-ICR kept good type I error control. These results suggest that precise capture of BOLD signals at the time series and component levels is a viable way to manage the deleterious effects of subject motion even at the group-level in terms of statistical error control.

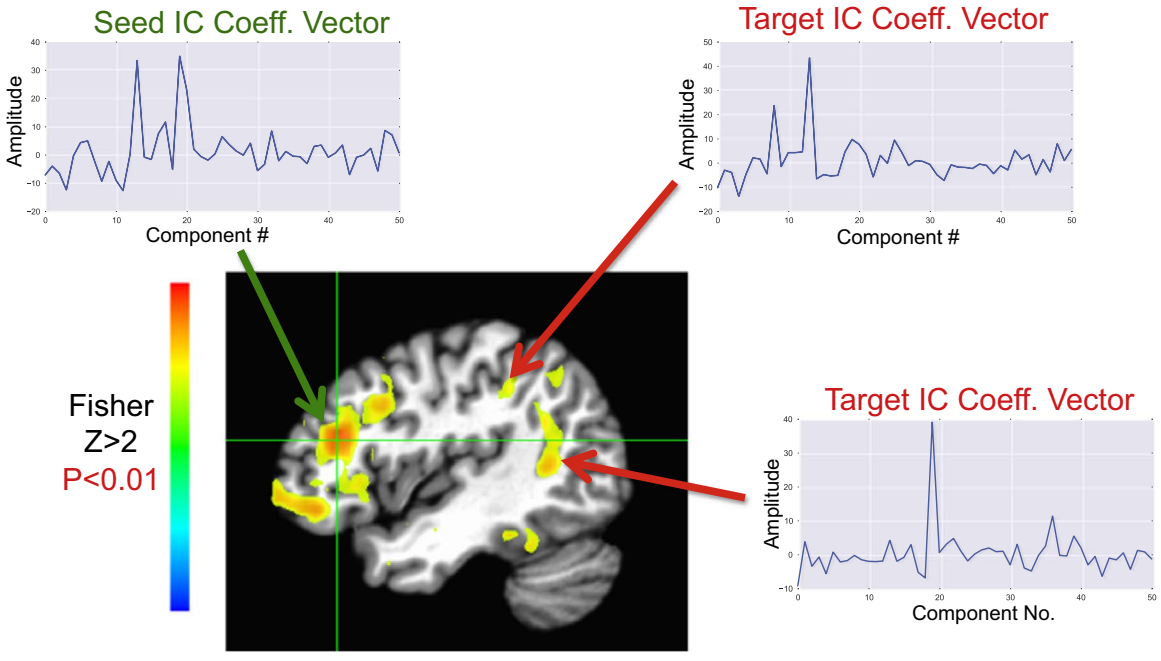

Fig. 14. Multi-echo independent coefficients regression (ME-ICR). At subject-level, after finding BOLD components, vectors of IC coefficients can be used to computed seed-based connectivity analysis. IC weights are independent, meaning ordinary least squares fits are suited to conventional statistical significance of connectivity estimates. Pearson correlations of IC vectors can be Fisher transformed to Z-values that factor in degrees of freedom.

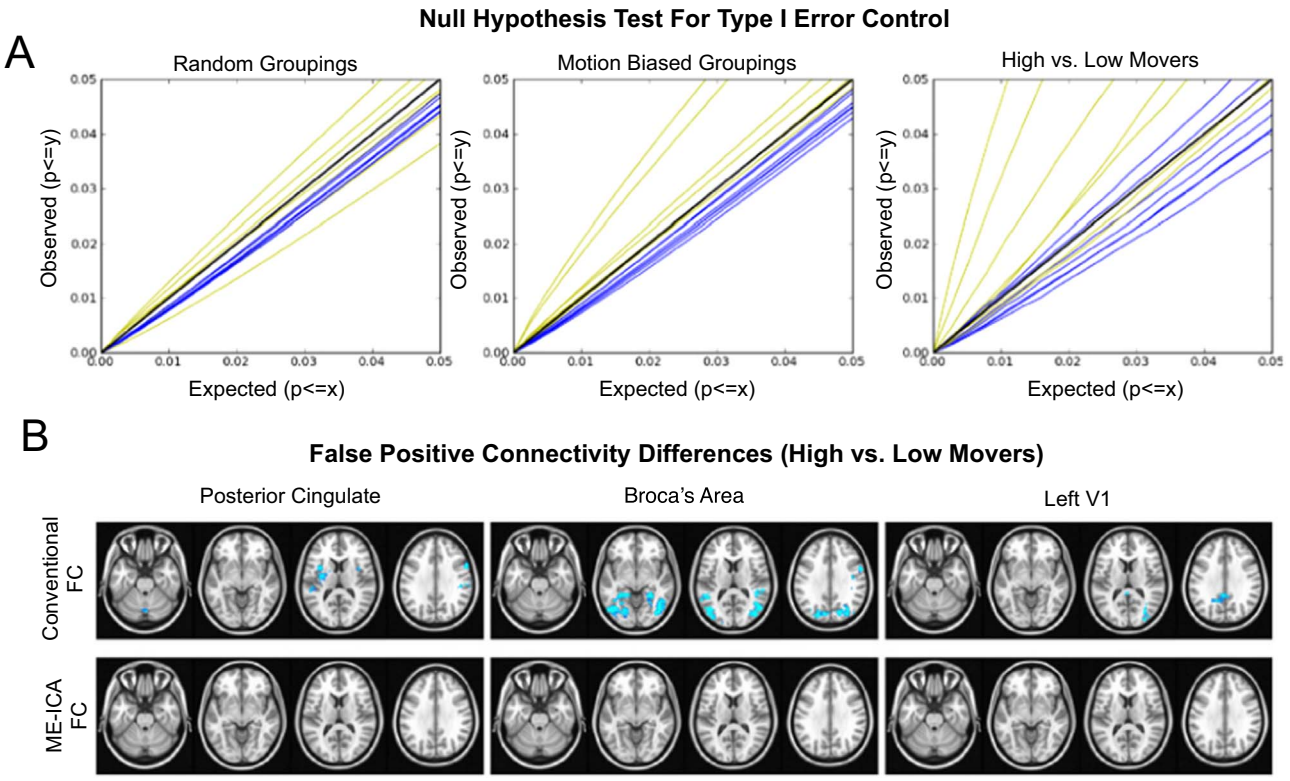

Fig. 15. (A) T-tests of seed-connectivity maps in various permuted subject groups based on level of subject head motion, for seven seeds. Over an average of 50 random groupings, both ME-ICR (blue) and conventional (yellow) connectivity have type I error that match the expected error (black). As groupings are biased by the level of head motion (50 permutations), conventional analysis shows doubled type I error. In contrast, ME-ICR shows good type I error control (50 permutations). For the single test of high versus low motion subjects based on median split, ME-ICR shows good type I error control, while conventional connectivity shows high type I error. (B) Regions that show connectivity differences due to type I error, after cluster correction. Adapted from Kundu et al. (2013).

ME-fMRI using MB EPI and 7 T MRI

A perceived cost of the ME approach relates to the investment of imaging time to acquire more echoes, instead of using imaging time to acquire at high resolution. On the one hand, high spatial resolution is important for localizing brain function precisely. On the other hand, smaller voxel size leads to lower per-voxel signal to noise ratio, lowering the odds of detecting weaker signals, such as in deep brain areas, despite high spatial resolution. In regards to temporal resolution, acquiring more echoes leads to longer TRs, which in turn means slower temporal sampling. A high temporal sampling rate for fMRI, on the other hand, can help reduce aliasing of signals from different sources such as networks and artifacts. Using standard single-slice EPI readouts and 3 T MRI, a target of a 2 s TR to capture brain volumes at 3 TEs at 3mm voxel size is achievable with low levels of in-plane acceleration while retaining good signal to noise ratio. These sequences have so far led to meaningful findings on brain function in health and disease (Morris et al., 2016a, 2016b). Acquiring ME-fMRI at much higher spatial resolution, which takes more time to image, will, however, lead to a mostly dephased last echo image, and will also require acceleration factors that lead to high imaging noise. For studies close to the level of cortical layers (Koopmans et al., 2011; Polimeni et al., 2010), higher resolution is needed, and so these applications necessitate major changes in hardware or acquisition strategy in order to utilize ME-fMRI. One way of increasing imaging speed while using standard EPI is using faster MRI gradients, as available with newer MRI platforms such as GE MR750 and Siemens Prisma. Another way is imaging at higher field strengths, namely 7 T MRI. This approach increases signal-to-noise ratio, which in turn supports higher in-plane acceleration and shorter image readout times. A very recent possibility is ME imaging with multiband (MB) acceleration. This approach speeds imaging by acquiring multiple EPI slices simultaneously. MB-EPI, in turn, reduces time to acquire volumes by integral factors, without changing slice read out times.

The first multi-echo multi-band (MEMB)-EPI sequence was implemented in Olafsson et al. (2015). This was done at 3 T, using the GE MRI 750 platform and a 32-channel head coil. One motivation was to enable MB-fMRI on the GE platform that could be compatible with the sequence on the Siemens platform used to acquire data compatible with the Human Connectome Project (HCP) (Van Essen et al., 2012). The GE MEMB sequence also enabled the option for concurrent in-plane and MB acceleration, that was not part of the HCP protocol. The in-plane acceleration mode, in turn, allows ME imaging since a late TE can be acquired before signals dephase to the noise floor. Comparing single-band and MEMB sequences is possible using the same slice configuration, with 3.75mm voxel size, but with respective TRs of 2.5 s versus 0.8 s after 3-fold MB acceleration. In this configuration, ME-ICA identifies significantly more BOLD-like components in the MEMB data as compared to data acquired with a conventional ME single-slice acquisition. This is attributed to greater fragmentation of larger scale networks into finer scale networks (Fig. 16), supporting the hypothesis that higher temporal sampling can lead to better-separated networks. An analysis of the effect of aliasing also shows improved performance of the MEMB method derived from both an increase in the number of temporal samples and the consequent ability to filter out high-frequency artifacts due to less temporal aliasing. There may also be additional benefits of MEMB-fMRI in removing artifacts in MB-EPI data due to "slice leakage" of high amplitude artifact into other slices of the MB slice group (Olafsson et al., 2015). Altogether, the ME approach can take advantage of MB acceleration to increase temporal resolution with positive benefits.

Achieving fMRI with high spatial resolution as well as good temporal signal to noise ratio remains challenging due to the basic detection limits determined by MRI field strength and other MRI

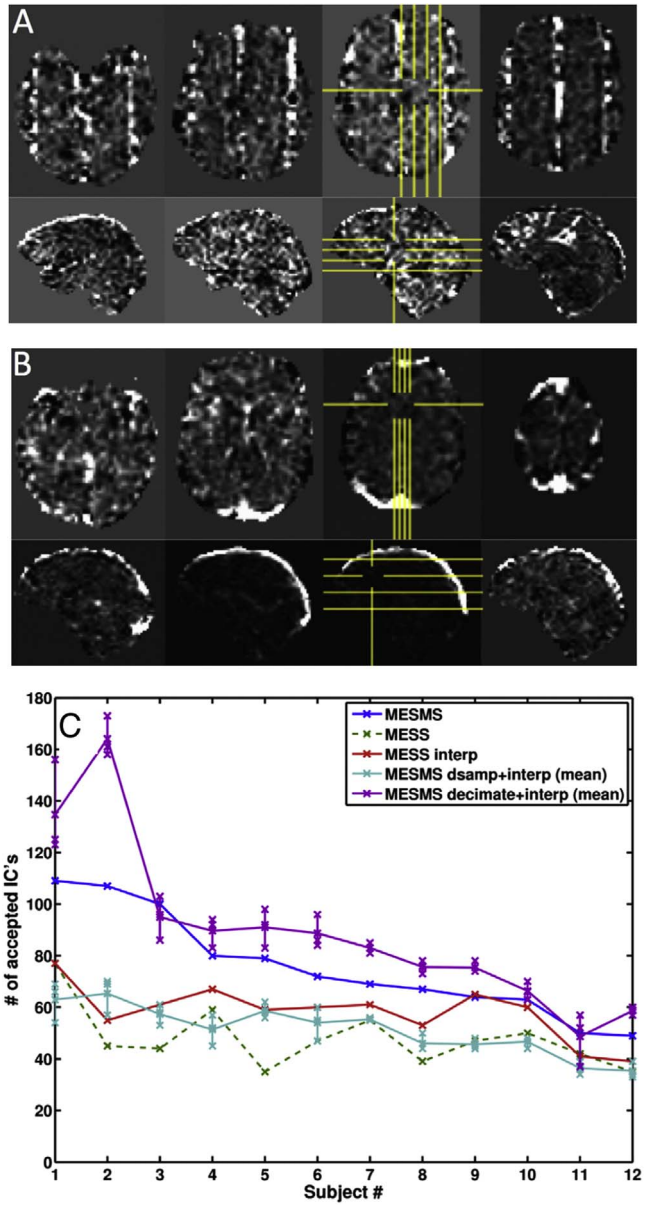

Fig. 16. Multi-echo simultaneous multi-slice (ME-SMS) fMRI. (A) Slice leakage artifact detected as a non-BOLD component; note sagittal acquisition. (B) Draining vein component detected as a non-BOLD component. (C) Number of BOLD components in ME-SMS versus multi-echo single slice (MESS) and various filtering steps. Upsampling MESS data to ME-SMS temporal resolution does not increase the number of BOLD components. Downsampling and interpolating ME-SMS data matches MESS in BOLD components. Decimating and interpolating ME-SMS approximates ME-SMS BOLD component count. This finding shows that high speed acquisition leads to more BOLD information in time series and less aliased signals. Decimating and upsampling may enhance BOLD network subdivision. Adapted from Olafsson et al. (2014).

hardware properties such as gradient performance. Nonetheless, high signal to noise ratio is key for optimal detection of BOLD signals. High field strength, such as 7 T, is an increasingly viable route to increasing BOLD sensitivity, as increased field strength leads to almost proportionally increased fMRI signal to noise ratio (Vaughan et al., 2001). However, fMRI acquired at high field strengths with single-echo fMRI can suffer high dropout due to high T_2* inhomogeneity. To address these and related issues, MEMB-EPI on 7 T MRI has become a viable option, as shown first on the Siemens Magnetom 7 T MRI platform (Boyacioğlu et al., 2015), using a multi-band factor of 3, in-plane acceleration factor 3, and acquiring 3 TEs. The combination of 7 T and ME imaging compensates for dropout and increases overall BOLD contrast after combining ME signals with the PAID method discussed previously. Boyacioğlu et al. used FSL MELODIC and the FSL FIX component selection approach (Salimi-Khorshidi et al., 2014), which is a template training-based selection procedure, and showed detection of multiple resting state networks. Networks of large anatomical extents such as relating to motor, language, and parietal cortices showed subdivisions into more specialized regions such as right and left lateralized network nodes. In an analysis of Stroop task activation, artifact components were regressed out of time series from the task runs, and task activation maps of the resulting data showed localization consistent with the Stroop activation based on the NeuroSynth atlas (Yarkoni et al., 2011). These results together suggest that fMRI using the combined MEMB approach could be superior to using standard single-echo multi-band EPI at 7 T.

In summary, to achieve faster volume imaging speed for multi-echo data, several hardware and pulse sequence approaches can be used, with multi-band EPI being highly promising. These approaches can moreover be combined, leading for example to MBME-fMRI, possible at 3 T and 7 T. However, it is yet to be fully determined which experimental conditions are better suited to acquiring fMRI with faster volume acquisition by forgoing multi-echo acquisition, or capturing and utilizing multi-echo information while imaging at slower imaging speed. It is important to note that ME-fMRI virtually necessitates parallel imaging acceleration, which has associated signal-to-noise penalty in individual TE time series. Further study is also needed to determine which combination of experimental design and acquisition is suited to which denoising approach, involving a multi-way comparison of single- versus multi-band and echo, and FSL FIX and ME-ICA. For instance, studies involving homogeneous samples of participants where functional and artifact components would be expected to be repeatable across subjects could benefit more from maximizing imaging speed and not spending time acquiring multiple echoes. However, in experimental designs where artifact patterns are more difficult to predict, such as those involving smaller cohorts, heterogeneous populations, or abnormal neuroanatomy - as associated to disease and clinical contexts - the cost-benefit assessment may favor the ME approach.

ME-fMRI of non-normative neuroanatomy

The use of ME-ICA at 7 T could make high-resolution fMRI studies possible for anatomies that are non-standard since ME-ICA needs no comparisons to standard anatomy to identify networks and artifacts. Fig. 17 demonstrates MEMB-fMRI with 2.5 mm isotropic voxel size with 4 TEs using 7 T MRI acquired from controls and epilepsy patients, analyzed with ME-ICA. For a 10-minute resting state dataset of a normal volunteer, representative BOLD networks are shown. Subcortical activity readily sub-divides into distinct areas such as dorsal and ventral striatum. The detection of ventral striatum is notable since it is localized to a region with high dropout due to short T_2*. A patient with focal epilepsy was imaged using the same sequence, and also with T2 FLAIR. T1 and T2 images show a dysembrogenic neuroepithelial tumor (DNET) in the right superior temporal lobe, affected by edema (dark area in Fig. 18). By playing high-κ BOLD time series as a dynamic movie, transient BOLD signals can be seen arising near the lesion, suggesting functional cortex. By computing connectivity from a region of interest of about 10 cubic millimeters in volume to the whole brain, aberrant connectivity can be seen to putamen and cerebellum. Further study can help to determine to what extent ME-ICA and MEMB-EPI at 7 T could be used for studying lesional cortex when both high spatial resolution and functional sensitivity is needed.

Making ME-fMRI practical

It might be surprising that with all the information to be gained from ME-fMRI over standard fMRI, ME-fMRI is still not standard. For

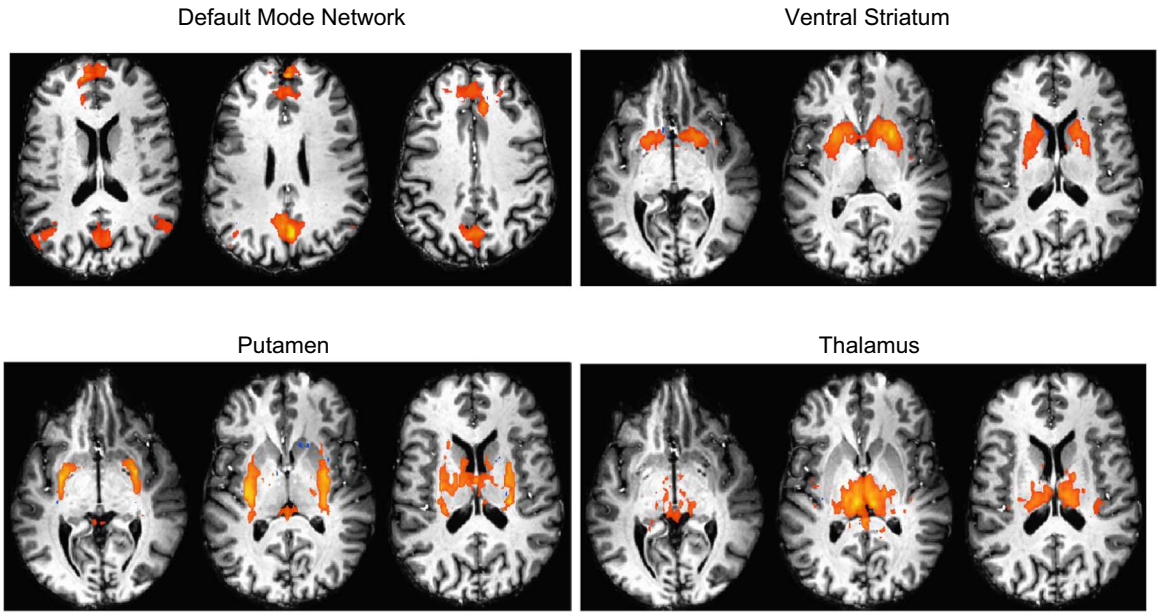

Fig. 17. Components from ME-ICA at 7 T MRI of healthy individual. Canonical cortical networks, such as the default mode network are found with good spatial resolution. In addition, subcortex is parcellated into functionally distinct networks, even at the individual-subject level.

example, the spiral and echo planar (SPEP) sequence by Wong et al., available for several years for the GE platform, could flexibly implement ME-fMRI as well as other techniques such as echo relaxation imaging. The main practical problem has been that gradient echo image readout takes too much time without in-plane acceleration so that by even a third TE most signal is dephased away. Vital to making ME-fMRI more practical is acquiring images with in-plane acceleration. This speeds up image readout so that three to five TEs of whole-brain signals can be acquired within a standard TR of 2–3 s. In combination with recent developments in multi-band imaging, many-fold smaller TRs are achievable. The first widespread use of multi-echo acquisition and analysis was done based on the Siemens platform, originating at the F.C. Donders Centre for Cognitive Neuroimaging (Nijmegen, Netherlands) Institute, and affiliated institutions. Despite many successful uses, further spread of the multi-echo approach has still been encumbered by challenges in managing the multi-TE time series. To handle these issues related to practicality, the analysis tool *meica.py* has been developed and distributed to help streamline multi-echo analysis, by handling all stages of basic and ICA-based ME analysis.

The design intent of *meica.py* is to make ME-fMRI processing as easy as possible, so that "raw" ME-fMRI data can be input, and fully processed BOLD time series and component maps are output. The pipeline is also meant to be flexible, so analysis can be done with or without an anatomical image, and in standard space or not. It is also open-source, in being based on the GPL licensed AFNI and Python tools for open science (available at www.bitbucket.org/prantikk/me-ica). There are two main steps for this pipeline. *meica.py* itself writes a shell script for preprocessing using AFNI tools. This adapts mostly basic fMRI preprocessing, but is applied with TE properties in mind, and is designed to keep multi-TE time series aligned. For example, the early TE data is used for rigid body motion correction on the basis of having highest signal intensity across tissues. Based on a sample of ME images from a short series of TRs, optimally combined signals are used to make a mask image by a variant of the BET method. Local Pearson correlation of T_2* with the anatomical drives functional-anatomical coregistration (Kundu et al., 2015). The parameters of motion correction and alignment are combined in one matrix and applied to all TE time series. Band pass filtering and spatial smoothing are not recommended but are supported. The script then calls another code, *tedana.py*, that implements several ME analyses such as T_2* model fitting and ICA, based on the equations in this manuscript. These functions are built with routines from the Numpy and Scipy Python toolkits. These implementations are efficient by virtue of passing computationally intense steps to optimized low-level and parallelized linear algebra codes built into Python toolkits. *tedana.py* first does ME-PCA to isolate signals for ICA, by default on optimally combined data. It then finds ICA components using FastICA, implemented with Numpy and Scipy routines. Each component is then processed to compute κ and ρ, and other accessory component metrics. These additional metrics aid in capturing specific artifacts such as from in-plane acceleration and draining veins. Last, components are classified into BOLD and non-BOLD groups and constituted into time series for various processing approaches.

ME-ICA writes three different time series datasets that vary by how strictly BOLD versus non-BOLD signals are retained, with a rationale based on end use (Fig. 19). First are the T_2*-weighted "optimally combined" time series, which can be a drop-in replacement for standard fMRI data, while benefitting from signal to noise ratio boosts of the T_2* weighted combination. This data represents all BOLD and non-BOLD signals, though, so they benefit from some denoising such as motion regression etc. to be useful in most cases.

The second time series have non-BOLD and mid-κ ICs removed, but retain i) thermal noise, ii) low variance ICs, iii) and ignored ICs. This data, called ME-DN, removes a large portion of nuisance variance through removing a small number of components, far fewer than the number of time points. In effect, good denoising is achieved with a relatively small loss in degrees of freedom. The ME-DN time series are the most efficiently denoised from ME-ICA and are well suited to voxel-wise general linear modeling (GLM) at the subject level. This is because ME-DN data optimize the balance of low noise and high degrees of freedom, which is crucial for finding significant effects on the basis of T-statistics. However, the number of degrees of freedom does vary across ME-DN datasets, so efforts should be made to account for this variate in subject-level and group-level analyses to avoid inflated test statistics and false positive findings. In general, the ME-DN data are a safe option for good denoising with many retained degrees of freedom and are the main choice for subject level model fitting if software does not support setting degrees of freedom manually.

The third option is BOLD time series recomposed only from BOLD

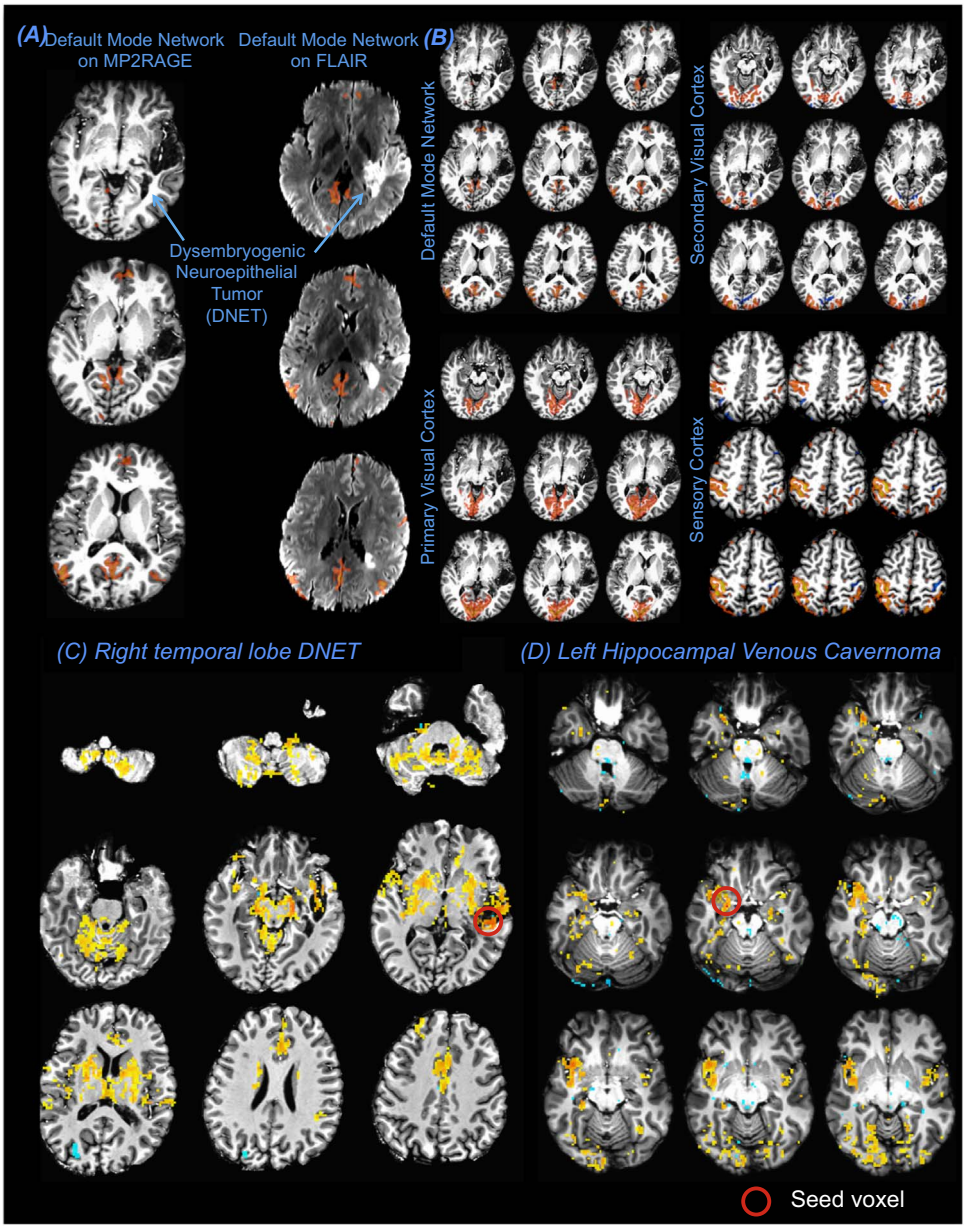

Fig. 18. ME-ICA of data from 7 T ME-fMRI of focal lesional epilepsy patients. (A) Default mode network of patient with dysembryonic neuroepithelial tumor (DNET), rendered on T1 and T2 MRI. (B) Other canonical functional networks of patient with DNET. (C) Seed-based functional connectivity of DNET lesion. Seed in parenchyma of lesion shows abnormal connectivity with putamen and cerebellum. (D) Seed connectivity for patient with venous cavernoma, with seed in hippocampus near abnormality. Connectivity is seen from seed region to ipsilateral superior temporal lobe and insula.

components. These time series, called the high-κ time series, have degrees of freedom equal to the number of BOLD components. High-κ data minimize the contribution of Gaussian noise, which is a special property. If these data are played as a video, they can show dynamic cortical waves of activity (Fig. 20). These data are also suitable for univariate task-based GLM analyses. However, T-statistics are not valid at subject-level if degrees of freedom are not carefully counted, which is not possible in most software. Nevertheless, GLM fit coefficients (β) computed from this data can be passed to group analysis such as using T-test or ANOVA without special considerations.

Other types of task activity that can be analyzed with ME-ICA is that from paradigms with very long blocks or other types of low-frequency patterns, with epochs on the order of minutes. This is not possible with single-echo fMRI due to the requirement of a high-pass filter to remove artifactual drift, which is non-specific and removes BOLD-related low-frequency fluctuations as well. The removal of drifts in multi-echo fMRI can be done by removing non-BOLD signals, which makes possible the detection of low-frequency activity related to BOLD contrast. More complex BOLD responses such as sigmoidal activations can also be detected (Fig. 21). Evans et al. (2015) evoked many such types of activity using visual stimuli with varying visual contrast. These activations were isolated and mapped based on ME-DN time series from ME-ICA. For several types of temporally complex activation models with very-low-frequency components including sigmoids, activations localized well to the visual cortex, as expected. The possibility of mapping ultra-low frequency fluctuations suggests an opportunity for future studies on the effects of drugs or learning to utilize the enhanced sensitivity to corresponding low-frequency signal changes. The findings also indicate the possibility to study much richer activity combining high and low frequencies. Mood induction using stimuli with emotional valence is one such example (Figs. 22 and 23).

Recent results suggest that ME-ICA can increase statistical power for detecting activation in standard experimental paradigms such as block designs. Lombardo et al. (2016) addressed the crisis of con-

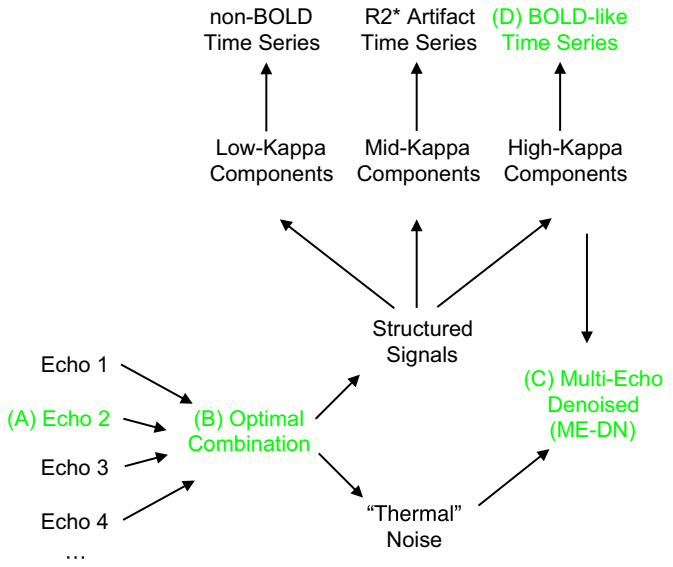

Fig. 19. Pipeline of component and time series outputs from ME-ICA. Key time series from multi-echo fMRI acquisition and ME-ICA analysis: (A) Time series of "middle" echo, can be used for standard fMRI analysis. (B) Time series after combining echoes, can be used for standard analysis. These time series have enhanced functional contrast and have compensated for dropout artifact. (C) Time series with non-BOLD artifact removed, but retaining Gaussian-like noise. (D) Time series from only BOLD components, suitable for studies of BOLD dynamics.

fidence of the statistical power of fMRI studies based on ME-fMRI of activation from two tasks from the 'theory of mind' domain. These tasks engage networks related to neural processing affected in the autism spectrum, borderline personality, and other disorders. To quantify the viability of signals of regions such as the anterior cingulate cortex (ACC), important for theory of mind tasks, power analysis was conducted based on the BOLD signals of the high-κ time series produced by ME-ICA. High-κ time series led to statistical power increases at a median rate of 27% over conventionally denoised T_2^* weighted time series in regions canonically associated with theory of mind activation (Fig. 22). Remarkably, 80% power for ACC activation was possible with cohorts of size N=12 versus N=45 for standard analysis. More substantial boosts (43–130%) were observed in non-canonical cerebellar areas. This finding newly suggests a role of subcortical areas in theory of mind processing. The effect size boosting was primarily a consequence of reducing non-BOLD noise at the subject level. It is key to note that, at group-level analysis, this reduction of non-BOLD noise also reduced between-subject variance. This finding indicated that the effect of noise on inter-subject variability in this sample was greater than the variability due to differences

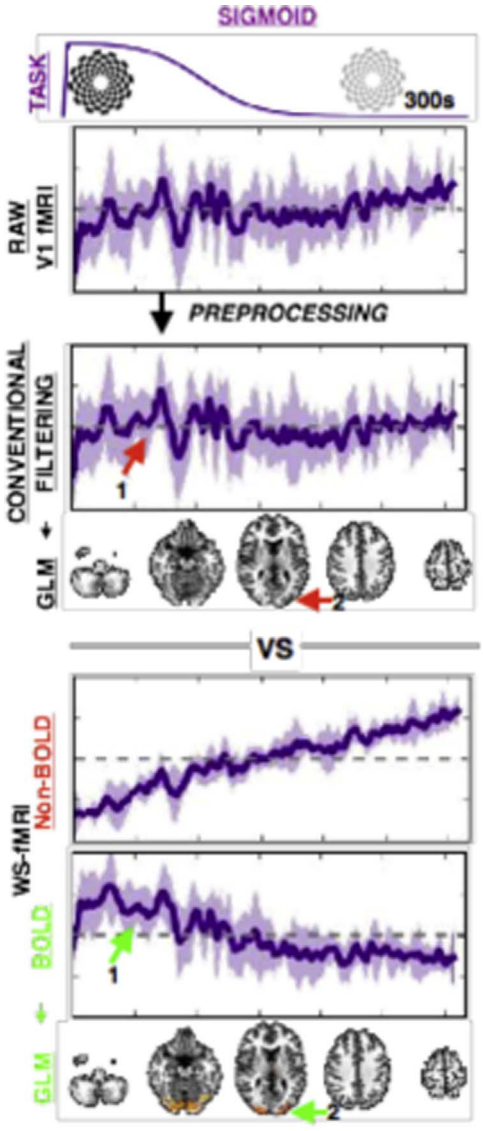

Fig. 21. Detection of sigmoidal BOLD effect after separating BOLD from non-BOLD signals. Raw fMRI from primary visual cortex during slow visual contrast change does not show slow BOLD change. Conventional time course filtering does not expose a slow varying effect. After ME-ICA, BOLD signal shows sigmoidal effect that localizes to visual cortex. Non-BOLD signal shows linear drift consistent with usual fMRI artifact. Adapted from Evans et al. (2015).

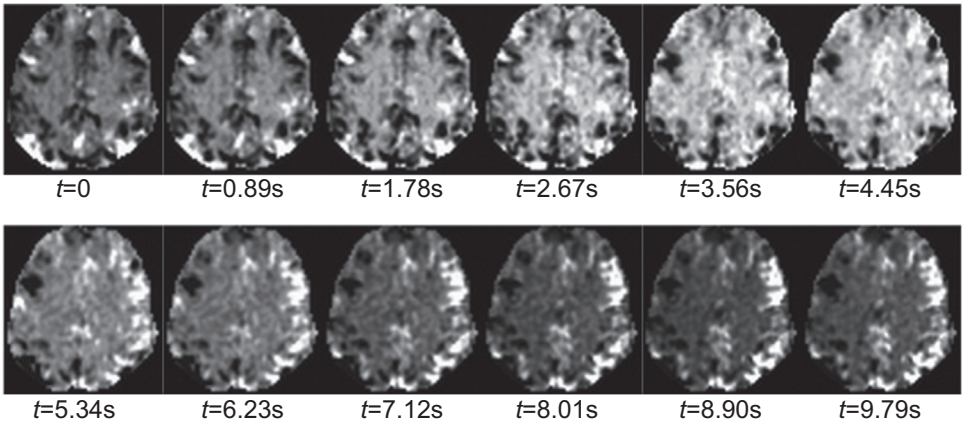

Fig. 20. Cortical dynamics captured in high-K time series. Using multi-echo multi-band fMRI sequence with in-plane acceleration factor (GRAPPA) 3, and multi-band factor 3, leading to 2.5 mm isotropic resolution sampled at TR=0.87 s. In evolution over about 10 s, the transition between two states of spontaneous activity states is seen.

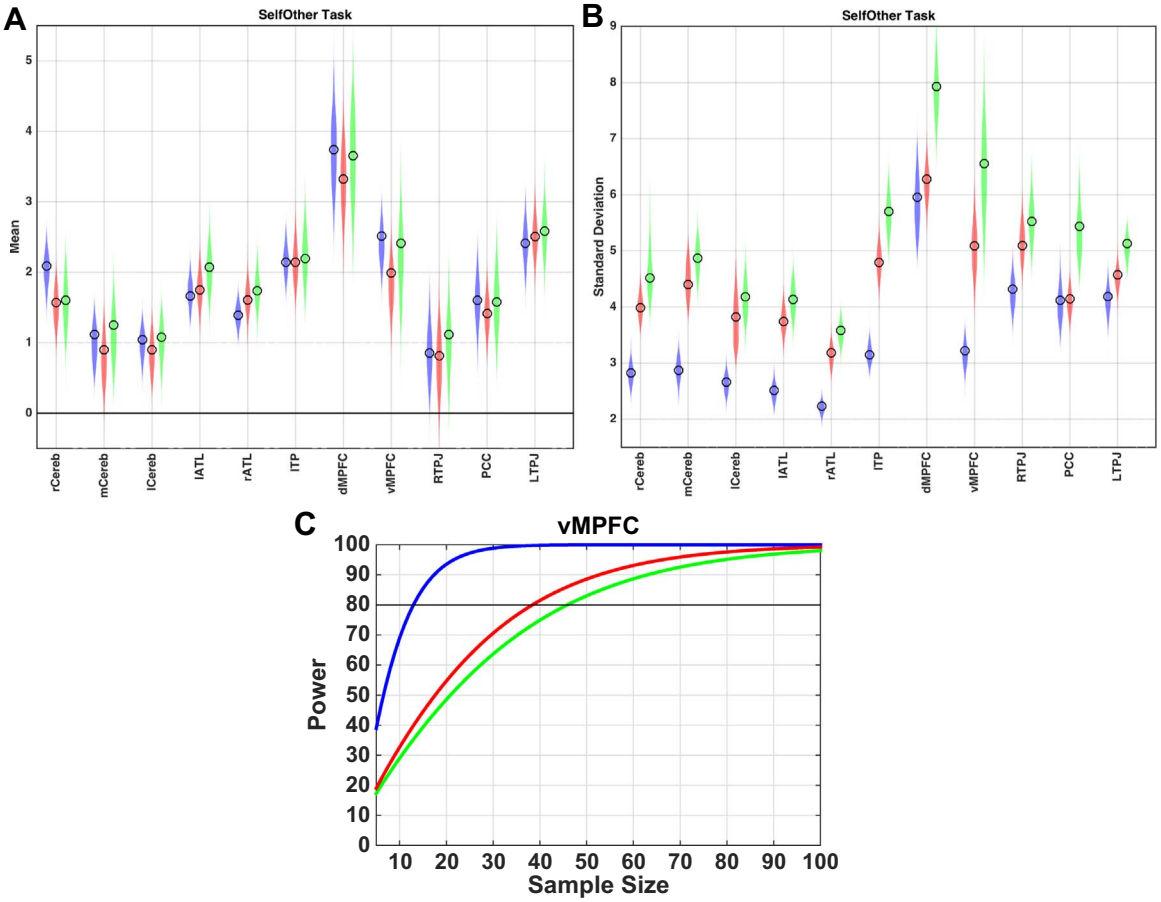

Fig. 22. Estimates of statistical power for an activation task of the mentalizing domain, sampled across several brain regions. Three methods are compared, including optimal combination and standard time series analysis, and GLMdenoise (Kay et al., 2013). (A) Mean activation is not different between different methods. (B) Inter-subject variability is considerably lower after ME-ICA denoising. (C) Power for detecting vmPFC activation is substantially higher for ME-ICA than other methods. Adapted from Lombardo et al. (2016).

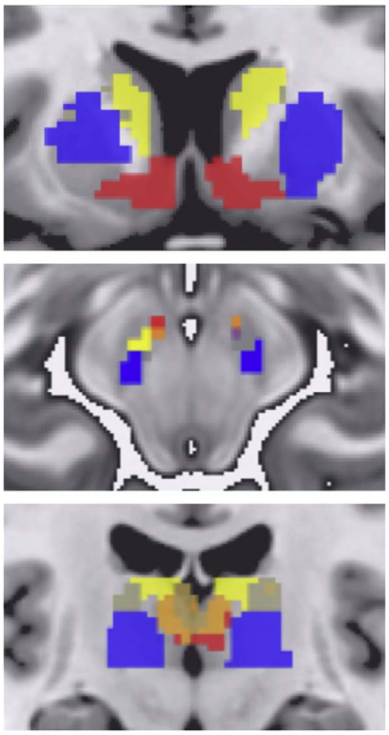

Fig. 23. Parcellation of thalamus and midbrain gray matter nuclei based on seed-based connectivity. Adapted from Morris et al. (2016a, 2016b).

in activation magnitudes. Removing non-BOLD noise thus led to large increases in power at the group-level for detecting activity in brain regions involved in theory of mind processing.

Greater statistical power due to less noisy data can be invested to find canonical effects in smaller groups, but also to find small effects in medium or large cohorts. Among signals that are of small effect size but crucial for study are those from the subcortex. Most fMRI research focuses on cortical activity, such as of the default mode network, partly part due to the lack of sensitivity in smaller areas such as in the subcortex. However, it is well known that pathogenic activity in neuropsychiatry relates strongly to subcortical areas. For instance, the striatum is linked to dopaminergic neurotransmission and is involved in Parkinson's disease, addiction, impulse control, and more. Moreover, subcortical areas link to each other and to the cerebral cortex in complex functional relationships. Morris et al., 2016 used resting state connectivity estimated from ME-fMRI data to map functional connectivity between striatum to multiple nodes in the cerebral cortex and subcortex for limbic, motor, and cognitive systems (Fig. 23). Limbic connectivity to striatum was shown for both ventromedial prefrontal cortex and ventral tegmentum, a small structure in the anterior midbrain. Motor connectivity was shown for the pre-supplementary motor area in cerebral cortex as well as the substantia nigra, a posterior lateral microstructure of the midbrain. Cortico-striatal connectivity was also shown to covary with behavioral scores for goal-direction, reversal learning, attentional shifting, and more. Thus, ME-ICA high-κ time series reflected both the anatomical connections and their functional differences of regions varying in size by orders of magnitude.

Conclusion

Over the history of the development of fMRI methods, ME-fMRI has been important in the process of validating BOLD-related origins of novel fMRI signal observations, such as resting state time series correlation. The need for validation of novel BOLD phenomena is due to the fact that only a fraction of variance captured in a typical fMRI experiment is related to BOLD contrast. Bandettini et al. and Peltier and Noll, separated by a few years, used highly targeted ME-fMRI applications to conduct these validation experiments. The use of ME-fMRI for validation purposes has not stopped, for instance, with Chen and Glover having recently used up-to-date MEMB methods to show that BOLD signals can span frequencies higher than the 0.2 Hz sampled by standard fMRI. The need to validate BOLD signals may indeed be growing, as new and complex artifacts are emerging at the same time as more demanding studies are being planned. As research questions and funding agencies focus on individual variation, high-fidelity BOLD at the subject level may also be important in efforts to increase statistical power. Newer uses of ME information may be well suited to studies of individual variation, with workflows like ME-ICA possibly helping to make fMRI-based discovery science a reality.

Current MRI systems using high-density head coils and fast gradients, along with parallel imaging, make ME-fMRI easier to acquire than ever before. The past limitations of ME-fMRI in regards to whole-brain coverage or standard resolutions are mostly gone, enabling its use in a wide range of fMRI studies. At present, ME-fMRI is available in research sequences from the authors covered in this review, on many current and upcoming scanners from major vendors (Olafsson et al., 2015; Poser et al., 2006). Emerging fMRI methods using multi-band acceleration and ultra-high field MRI may further make the ME approach attractive, and help counter new artifacts in more demanding studies, such as at 7 T (Boyacioğlu et al., 2014). Here we have reviewed recent ME-fMRI findings from studies in rest and task, animal and human, health and disease, 3 T and 7 T MRI, and with single-band and MB sequences. However, it is clear that acquiring ME-fMRI just for combination to compensate for signal dropout has major benefits for studies of regions such as orbitofrontal cortex and striatum, key in neuropsychiatry (Kirilina et al., 2016).

Much work does remain on further validating signals after ME-ICA and related processing. Using methods like spatial ICA beyond just component mapping and more for denoising needs care for factors like degrees of freedom in denoised data. Standard fMRI software for activation and correlation mapping may not be optimized for analysis of data that are denoised by removing variable numbers of components in an unaccounted way. Also, as data deviate farther from the smooth temporal fluctuations of the resting state or block design tasks and more to complex event-related designs, the configuration of processes like PCA and ICA become more pivotal. From using ME-ICA we find that higher estimates of data dimensionality may help in separating complex BOLD signals and artifact while keeping a stable ICA. Along these lines, further study is needed on how well physiological signals are removed with ICA-based methods such as ME-ICA or FSL MELODIC and FIX. Regarding the interaction of acquisition and analysis methods, it is interesting to note that an early motivating factor for the development and use of MB-fMRI was to sample signals and remove of cardiac pulsation, at around 1 Hz (Feinberg et al., 2010). In practice, such artifacts have been removed with spatial ICA, which does not use temporal patterns in the strict sense. Instead, a set of spatial patterns after dimensionality reduction is the basis of finding these artifacts. Thus, high sampling rate mainly supports more data dimensions for denoising. Moving forward with advanced fMRI methods, especially in making clinical inferences, it will be vital to make careful considerations of the imaging statistics that motivate acquisition and analysis. With an ME-fMRI approach, there exists the possibility to guide statistics with ‘physical’ signal models, as we demonstrated in ME-ICA results.

Studies on the statistical power for mapping various brain activity based on ME-fMRI have so far supported the notion that added information across TEs enhances group-level fMRI. Another recent issue of power in group-level fMRI activation mapping is how to best estimate the significance of clusters of voxels that pass per-voxel threshold tests (Eklund et al., 2016). The recommendation so far given existing data and tools comes down to using stricter cluster significance and making group inference by permutation test (Eklund et al., 2016). However, looming issues include how to study regions that are smaller than the smoothness factor of images, such as in subcortex, especially when data are smoothed outright to reduce noise as in standard fMRI. An ME method like ME-ICA has enhanced contrast from combining echoes, isolates noise components based on physical signal modes, and does not use explicit smoothing. These features suggest that the ME approach may be beneficial in tackling emerging issues of statistical power in task-related as well as resting state data.

Acquiring fMRI with multiple echoes has up-front costs of resolution, at least nominally. As discussed, though, with specific isolation of BOLD and non-BOLD signals as well as thermal noise extended fMRI preprocessing steps are made less crucial, which lessens the chance of related confounds. Of special interest is that the ME approach may newly enable or greatly ease the implementation of new kinds of fMRI experiments, that would be very challenging if using standard fMRI. For instance, experiments where activation spans both fast and slow signal effects, as could happen in event-related neural adaptation paradigms, are likely to be facilitated by ME-fMRI approaches. Detecting slow changes related to drugs may also be facilitated by the ME-fMRI approach, but more work is needed to establish this application.

BOLD fMRI has long been remarkable in revealing quite specific information about brain organization in a totally non-invasive way. At the same time, as experiments become more sophisticated and require fMRI methods that have higher sensitivity to BOLD signal and greater resilience to noise, a simple but universal fMRI signal model such as TE-dependence could be increasingly vital. As it has before, ME-fMRI may have a key role in future discoveries in fMRI.

Acknowledgements

PK and PB are supported by the Icahn School of Medicine Capital Campaign, the Translational and Molecular Imaging Institute, Brain Imaging Center and the Department of Radiology at the Icahn School of Medicine. PB is supported by funding from NIH-NCI (R01 CA202911) and NIH-NIMH (R01 MH109544) and Siemens Healthcare. VV is a Wellcome Trust Intermediate Fellow in Clinical Neurosciences (093705/Z/10/Z). We would like to thank Drs. Lara V. Marcuse and Madeline Fields at the Mount Sinai Epilepsy Center for their critical contributions towards imaging epilepsy patients in 7 T MRI. We would also like to thank Drs. Ed Bullmore and Souheil Inati for many important discussions on statistical and biophysical modelling of multi-echo fMRI signals.

References

Aguirre, G.K., Detre, J.A., 2012. The development and future of perfusion fMRI for dynamic imaging of human brain activity. NeuroImage 62, 1279–1285. http://dx.doi.org/10.1016/j.neuroimage.2012.04.039.

Bandettini, P., Wong, E., Hinks, R., Tikofsky, R., Hyde, J., 1992. Time course EPI of human brain function during task activation. Magn. Reson. Med. 25, 390–397.

Bandettini, P.A., Wong, E.C., Jesmanowicz, A., Hinkst, R.S., Hyde, J.S., 1994. Spin-echo and graciient-E brain activation using BOLD a comparative study at 1.5 T. NMR Biomed. 7, 12–20.

Beckmann, C., Smith, S., 2004. Probabilistic independent component analysis for functional magnetic resonance imaging. IEEE Trans. Med. Imaging 23, 137–152.

Bell, A., Sejnowski, T., 1995. An information-maximization approach to blind separation and blind deconvolution. Neural Comput. 7, 1129–1159.

Boyacioğlu, R., Schulz, J., Koopmans, P.J., Barth, M., Norris, D.G., 2015. Improved sensitivity and specificity for resting state and task fMRI with multiband multi-echo EPI compared to multi-echo EPI at 7 T. NeuroImage 119, 352–361. http://

dx.doi.org/10.1016/j.neuroimage.2015.06.089.
Boyacioğlu, R., Schulz, J., Müller, N.C.J., Koopmans, P.J., Barth, M., Norris, D.G., 2014. Whole brain, high resolution multiband spin-echo EPI fMRI at 7 T: a comparison with gradient-echo EPI using a color-word Stroop task. NeuroImage 97, 142–150. http://dx.doi.org/10.1016/j.neuroimage.2014.04.011.
Bright, M.G., Murphy, K., 2015. Is fMRI "noise" really noise? Resting state nuisance regressors remove variance with network structure. NeuroImage 114, 158–169. http://dx.doi.org/10.1016/j.neuroimage.2015.03.070.
Bright, M.G., Murphy, K., 2013. Removing motion and physiological artifacts from intrinsic BOLD fluctuations using short echo data. NeuroImage 64, 526–537. http://dx.doi.org/10.1016/j.neuroimage.2012.09.043.
Bullmore, E., Brammer, M., Williams, S.C., Rabe-Hesketh, S., Janot, N., David, A., Mellers, J., Howard, R., Sham, P., 1996. Statistical methods of estimation and inference for functional MR image analysis. Magn. Reson. Med. 35, 261–277.
Bullmore, E., Fadili, J., Maxim, V., Sendur, L., Whitcher, B., Suckling, J., Brammer, M., Breakspear, M., 2004. Wavelets and functional magnetic resonance imaging of the human brain. NeuroImage 23 (Suppl 1), S234–S249.
Button, K.S., Ioannidis, J.P.A., Mokrysz, C., Nosek, B.A., Flint, J., Robinson, E.S.J., Munafò, M.R., 2013. Power failure: why small sample size undermines the reliability of neuroscience. Nat. Rev. Neurosci. 14, 365–376. http://dx.doi.org/10.1038/nrn3475.
Buur, P.F., Norris, D.G., Hesse, C.W., 2008. Extraction of task-related activation from multi-echo BOLD fMRI. IEEE J. Sel. Top. Signal Process. 2, 954–964.
Buur, P.F., Poser, B.A., Norris, D.G., 2009. A dual echo approach to removing motion artefacts in fMRI time series. NMR Biomed. 22, 551–560.
Buxton, R.B., Wong, E.C., Frank, L.R., 1998. Dynamics of blood flow and oxygenation changes during brain activation: the balloon model. Magn. Reson. Med. 39, 855–864.
Carp, J., 2013. Optimizing the order of operations for movement scrubbing: comment on Power et al. NeuroImage 76, 436–438. http://dx.doi.org/10.1016/j.neuroimage.2011.12.061.
Chen, J.E., Glover, G.H., 2015. BOLD fractional contribution to resting-state functional connectivity above 0.1 Hz. NeuroImage 107, 207–218. http://dx.doi.org/10.1016/j.neuroimage.2014.12.012.
Correa, N., Adalı, T., Calhoun, V.D., 2007. Performance of blind source separation algorithms for fMRI analysis using a group ICA method. Magn. Reson. Imaging 25, 684–694. http://dx.doi.org/10.1016/j.mri.2006.10.017.
Deichmann, R., Josephs, O., Hutton, C., Hutton, D.R., Turner, R., 2002. Compensation of susceptibility-Induced BOLD sensitivity losses in echo-planar fMRI imaging. NeuroImage 15, 120–135.
Eklund, A., Nichols, T.E., Knutsson, H., 2016. Cluster failure: why fMRI inferences for spatial extent have inflated false-positive rates. Proc. Natl. Acad. Sci. 113, 7900–7905. http://dx.doi.org/10.1073/pnas.1602413113.
Evans, J.W., Kundu, P., Horovitz, S.G., Bandettini, P.A., 2015. Separating slow BOLD from non-BOLD baseline drifts using multi-echo fMRI. NeuroImage 105, 189–197. http://dx.doi.org/10.1016/j.neuroimage.2014.10.051.
Fair, D.A., Cohen, A.L., Power, J.D., Dosenbach, N.U.F., Church, J.A., Miezin, F.M., Schlaggar, B.L., Petersen, S.E., 2009. Functional brain networks develop from a "local to distributed" organization. PLoS Comput. Biol. 5, e1000381.
Feinberg, D.A., Moeller, S., Smith, S.M., Auerbach, E., Ramanna, S., Glasser, M.F., Miller, K.L., Ugurbil, K., Yacoub, E., 2010. Multiplexed echo planar imaging for sub-second whole brain FMRI and fast diffusion imaging. PLoS One 5, e15710.
Fox, M.D., Zhang, D., Snyder, A.Z., Raichle, M.E., 2009. The global signal and observed anticorrelated resting state brain networks. J. Neurophysiol. 101, 3270–3283.
Friston, K.J., Holmes, A.P., Poline, J., Grasby, P., Williams, S., Frackowiak, R.S.J., Turner, R., 1995. Analysis of fMRI time-series revisited. Neuroimage 2, 45–53.
Glover, G., Li, T., Ress, D., 2000. Image based method for retrospective correction of physiological motion effects in fMRI: retroicor. Magn. Reson. Med. 44, 162–167.
Gonzalez-Castillo, J., Panwar, P., Buchanan, L.C., Caballero-Gaudes, C., Handwerker, D.A., Jangraw, D.C., Zachariou, V., Inati, S., Roopchansingh, V., Derbyshire, J.A., Bandettini, P.A., 2016. Evaluation of multi-echo ICA denoising for task based fMRI studies: block designs, rapid event-related designs, and cardiac-gated fMRI. NeuroImage 141, 452–468. http://dx.doi.org/10.1016/j.neuroimage.2016.07.049.
Gowland, P., Bowtell, R., 2007. Theoretical optimization of multi-echo fMRI data acquisition. Phys. Med. Biol 52, 1801.
Hampson, M., Peterson, B.S., Skudlarski, P., Gatenby, J.C., Gore, J.C., 2002. Detection of functional connectivity using temporal correlations in MR images. Hum. Brain Mapp. 15, 247–262. http://dx.doi.org/10.1002/hbm.10022.
Hyvarinen, A., 1999. Fast and robust fixed-point algorithms for independent component analysis. IEEE Trans. Neural Netw. 10, 626–634.
Ing, A., Schwarzbauer, C., 2012. A dual echo approach to motion correction for functional connectivity studies. NeuroImage 63, 1487–1497. http://dx.doi.org/10.1016/j.neuroimage.2012.07.042.
Jo, H.J., Saad, Z.S., Simmons, W.K., Milbury, L.A., Cox, R.W., 2010. Mapping sources of correlation in resting state FMRI, with artifact detection and removal. NeuroImage 52, 571–582.
Kay, K.N., Rokem, A., Winawer, J., Dougherty, R.F., Wandell, B.A., 2013. GLMdenoise: a fast, automated technique for denoising task-based fMRI data. Front. Neurosci. 7.
Kirilina, E., Lutti, A., Poser, B.A., Blankenburg, F., Weiskopf, N., 2016. The quest for the best: the impact of different EPI sequences on the sensitivity of random effect fMRI group analyses. NeuroImage 126, 49–59. http://dx.doi.org/10.1016/j.neuroimage.2015.10.071.
Koopmans, P.J., Barth, M., Orzada, S., Norris, D.G., 2011. Multi-echo fMRI of the cortical laminae in humans at 7 T. NeuroImage 56, 1276–1285. http://dx.doi.org/10.1016/j.neuroimage.2011.02.042.
Krüger, G., Glover, G.H., 2001. Physiological noise in oxygenation sensitive magnetic resonance imaging. Magn. Reson. Med. 46, 631–637.
Kundu, P., Benson, B.E., Baldwin, K.L., Rosen, D., Luh, W.-M., Bandettini, P.A., Pine, D.S., Ernst, M., 2015. Robust resting state fMRI processing for studies on typical brain development based on multi-echo EPI acquisition. Brain Imaging Behav. 9, 56–73. http://dx.doi.org/10.1007/s11682-014-9346-4.
Kundu, P., Brenowitz, N.D., Voon, V., Worbe, Y., Vértes, P.E., Inati, S.J., Saad, Z.S., Bandettini, P.A., Bullmore, E.T., 2013. Integrated strategy for improving functional connectivity mapping using multiecho fMRI. Proc. Natl. Acad. Sci., 201301725.
Kundu, P., Inati, S.J., Evans, J.W., Luh, W.-M., Bandettini, P.A., 2012. Differentiating BOLD and non-BOLD signals in fMRI time series using multi-echo EPI. NeuroImage 60, 1759–1770. http://dx.doi.org/10.1016/j.neuroimage.2011.12.028.
Kundu, P., Inati, S.J., Evans, J.W., Luh, W.M., Bandettini, P.A., 2011. Differentiating BOLD and non-BOLD signals in fMRI time series using multi-echo EPI. NeuroImage.
Kundu, P., Santin, M.D., Bandettini, P.A., Bullmore, E.T., Petiet, A., 2014. Differentiating BOLD and non-BOLD signals in fMRI time series from anesthetized rats using multi-echo EPI at 11.7 T. NeuroImage 102 (Pt 2), 861–874. http://dx.doi.org/10.1016/j.neuroimage.2014.07.025.
Lombardo, M.V., Auyeung, B., Holt, R.J., Waldman, J., Ruigrok, A.N.V., Mooney, N., Bullmore, E.T., Baron-Cohen, S., Kundu, P., 2016. Improving effect size estimation and statistical power with multi-echo fMRI and its impact on understanding the neural systems supporting mentalizing. NeuroImage.
McKeown, M.J., Hu, Y., Wang, Z.J., 2005. ICA denoising for event-related fMRI studies. Presented at the engineering in medicine and biology society, 2005. In: Proceedings of the 27th Annual International Conference of the IEEE-EMBS 2005, IEEE, pp. 157–161.
Menon, R.S., Ogawa, S., Hu, X., Strupp, J.P., Anderson, P., Uurbil, K., 1995. BOLD based functional MRI at 4 T includes a capillary bed contribution: echo planar imaging correlates with previous optical imaging using intrinsic signals. Magn. Reson. Med. 33, 453–459.
Morris, L.S., Kundu, P., Baek, K., Irvine, M.A., Mechelmans, D.J., Wood, J., Harrison, N.A., Robbins, T.W., Bullmore, E.T., Voon, V., 2016a. Jumping the gun: mapping neural correlates of waiting impulsivity and relevance across alcohol misuse. Biol. Psychiatry 79, 499–507. http://dx.doi.org/10.1016/j.biopsych.2015.06.009.
Morris, L.S., Kundu, P., Dowell, N., Mechelmans, D.J., Favre, P., Irvine, M.A., Robbins, T.W., Daw, N., Bullmore, E.T., Harrison, N.A., Voon, V., 2016b. Fronto-striatal organization: defining functional and microstructural substrates of behavioural flexibility. Cortex J. Devoted Study Nerv. Syst. Behav. 74, 118–133. http://dx.doi.org/10.1016/j.cortex.2015.11.004.
Murphy, K., Birn, R.M., Handwerker, D.A., Jones, T.B., Bandettini, P.A., 2009. The impact of global signal regression on resting state correlations: are anti-correlated networks introduced? NeuroImage 44, 893–905. http://dx.doi.org/10.1016/j.neuroimage.2008.09.036.
Ogawa, S., Lee, T.M., Kay, A.R., Tank, D.W., 1990. Brain magnetic resonance imaging with contrast dependent on blood oxygenation. Proc. Natl. Acad. Sci. USA 87, 9868–9872.
Olafsson, V., Kundu, P., Wong, E.C., Bandettini, P.A., Liu, T.T., 2015. Enhanced identification of BOLD-like components with multi-echo simultaneous multi-slice (MESMS) fMRI and multi-echo ICA. NeuroImage 112, 43–51. http://dx.doi.org/10.1016/j.neuroimage.2015.02.052, Cyprus.
Peltier, S.J., Noll, D.C., 2000. Analysis of fMRI signal and noise component TE dependence. Neuroimage 11, S623.
Polimeni, J.R., Fischl, B., Greve, D.N., Wald, L.L., 2010. Laminar analysis of 7 T BOLD using an imposed spatial activation pattern in human V1. NeuroImage 52, 1334–1346. http://dx.doi.org/10.1016/j.neuroimage.2010.05.005.
Poser, B.A., Versluis, M.J., Hoogduin, J.M., Norris, D.G., 2006. BOLD contrast sensitivity enhancement and artifact reduction with multiecho EPI: parallel acquired inhomogeneity desensitized fMRI. Magn. Reson. Med. 55, 1227–1235.
Posse, S., Wiese, S., Gembris, D., Mathiak, K., Kessler, C., Grosse-Ruyken, M., Elghahwagi, B., Richards, T., Dager, S., Kiselev, V., 1999. Enhancement of BOLD-contrast sensitivity by single-shot multi-echo functional MR imaging. Magn. Reson. Med. 42, 87–97.
Power, J.D., Barnes, K.A., Snyder, A.Z., Schlaggar, B.L., Petersen, S.E., 2012. Spurious but systematic correlations in functional connectivity MRI networks arise from subject motion. Neuroimage 59, 2142–2154.
Saad, Z.S., Glen, D.R., Chen, G., Beauchamp, M.S., Desai, R., Cox, R.W., 2009. A new method for improving functional-to-structural MRI alignment using local Pearson correlation. Neuroimage 44, 839–848.
Salimi-Khorshidi, G., Douaud, G., Beckmann, C.F., Glasser, M.F., Griffanti, L., Smith, S.M., 2014. Automatic denoising of functional MRI data: combining independent component analysis and hierarchical fusion of classifiers. NeuroImage 90, 449–468. http://dx.doi.org/10.1016/j.neuroimage.2013.11.046.
Satterthwaite, T.D., Elliott, M.A., Gerraty, R.T., Ruparel, K., Loughead, J., Calkins, M.E., Eickhoff, S.B., Hakonarson, H., Gur, R.C., Gur, R.E., 2012. An improved framework for confound regression and filtering for control of motion artifact in the preprocessing of resting-state functional connectivity data. Neuroimage.
Smith, S., Jenkinson, M., Woolrich, M., Beckmann, C., Behrens, T., Johansen-Berg, H., Bannister, P., De Luca, M., Drobnjak, I., Flitney, D., 2004. Advances in functional and structural MR image analysis and implementation as FSL. Neuroimage 23, S208–S219.
Speck, O., Ernst, T., Chang, L., 2001. Biexponential modeling of multigradient-echo MRI data of the brain. Magn. Reson. Med. 45, 1116–1121. http://dx.doi.org/10.1002/mrm.1147.
Speck, O., Hennig, J., 1998. Functional imaging by I0 and T2* parameter mapping using multi image EPI. Magn. Reson. Med. 40, 243–248.
Thomas, C.G., Harshman, R.A., Menon, R.S., 2002. Noise reduction in BOLD-based

fMRI using component analysis. Neuroimage 17, 1521–1537.
Van Essen, D.C., Ugurbil, K., Auerbach, E., Barch, D., Behrens, T.E.J., Bucholz, R., Chang, A., Chen, L., Corbetta, M., Curtiss, S.W., Della Penna, S., Feinberg, D., Glasser, M.F., Harel, N., Heath, A.C., Larson-Prior, L., Marcus, D., Michalareas, G., Moeller, S., Oostenveld, R., Petersen, S.E., Prior, F., Schlaggar, B.L., Smith, S.M., Snyder, A.Z., Xu, J., Yacoub, E., WU-Minn HCP Consortium, 2012. The human connectome project: a data acquisition perspective. NeuroImage 62, 2222–2231. http://dx.doi.org/10.1016/j.neuroimage.2012.02.018.
Vaughan, J.T., Garwood, M., Collins, C.M., Liu, W., DelaBarre, L., Adriany, G., Andersen, P., Merkle, H., Goebel, R., Smith, M.B., Ugurbil, K., 2001. 7 T vs. 4 T: rf power, homogeneity, and signal-to-noise comparison in head images. Magn. Reson. Med. 46, 24–30. http://dx.doi.org/10.1002/mrm.1156.
Wang, D.J.J., Chen, Y., Fernandez-Seara, M.A., Detre, J.A., 2011. Potentials and challenges for arterial spin labeling in pharmacological magnetic resonance imaging. J. Pharmacol. Exp. Ther. 337, 359–366. http://dx.doi.org/10.1124/jpet.110.172577.
Wink, A.M., Roerdink, J.B.T.M., 2006. BOLD noise assumptions in fMRI. Int. J. Biomed. Imaging 2006, 1–11. http://dx.doi.org/10.1155/IJBI/2006/12014.
Yarkoni, T., Poldrack, R.A., Nichols, T.E., Van Essen, D.C., Wager, T.D., 2011. Large-scale automated synthesis of human functional neuroimaging data. Nat. Methods 8, 665–670.
Zhao, F., Wang, P., Hendrich, K., Ugurbil, K., Kim, S.-G., 2006. Cortical layer-dependent BOLD and CBV responses measured by spin-echo and gradient-echo fMRI: insights into hemodynamic regulation. Neuroimage 30, 1149–1160. http://dx.doi.org/10.1016/j.neuroimage.2005.11.013.